Meteoritics & Planetary Science 44, Nr 5, 665–687 (2009)
Abstract available online at http://meteoritics.org

The formation of boundary clinopyroxenes and associated glass veins in type B1 CAIs

J. M. PAQUE[1*], J. R. BECKETT[1], H. A. ISHII[2], A. ALÉON-TOPPANI[2, 3], D. S. BURNETT[1], N. TESLICH[2], Z. R. DAI[2], and J. P. BRADLEY[2]

[1]Division of Geological and Planetary Sciences, California Institute of Technology, Pasadena, California 91125, USA
[2]Institute of Geophysics and Planetary Physics, Lawrence Livermore National Laboratory, Livermore, California 94550, USA
[3]Institut d'Astrophysique Spatiale, Université Paris-Sud, Bât 121, 91405 Orsay Cedex, France
*Corresponding author. E-mail: julie@paque.com

(Received 03 June 2008; revision accepted 13 February 2009)

Abstract–We used focused ion beam thin section preparation and scanning transmission electron microscopy (FIB/STEM) to examine the interfacial region between spinel and host melilite for spinel grains in type B1 inclusions from the Allende and Leoville carbonaceous chondrites. Boundary clinopyroxenes decorating spinel surfaces have compositions similar to those of coarser clinopyroxenes from the same region of the inclusion, suggesting little movement after formation. Host melilite displays no anomalous compositions near the interface and late-stage minerals are not observed, suggesting that boundary pyroxenes did not form by crystallization of residual liquid. Allende spinels display either direct spinel-melilite contact or an intervening boundary clinopyroxene between the two phases. Spinel-melilite interfacial regions in a Leoville B1 are more complex, with boundary clinopyroxene, as observed in Allende, but also variable amounts of glass, secondary calcite, perovskite, and an Mg-, Al-, OH-rich and Ca-, Si-poor crystalline phase that may be a layered double hydrate. One possible scenario of formation for the glass veins is that open system alteration of melilite produced a porous, hydrated aggregate of Mg-carpholite or sudoite + aluminous diopside that was shock melted and quenched to a glass. The hydrated crystalline phase we observed may have been a shocked remnant of the precursor phase assemblage, but is more likely to have formed later by alteration of the glass.

In the mantle, boundary clinopyroxenes may have been crystallized from Ti-rich liquids formed by the direct dissolution of perovskite and an associated Sc-Zr-rich phase or as a reaction product between dissolving perovskite and liquid. In the core, any perovskite and associated Ti-enriched liquids that may have originally been present disappeared before the growth of boundary clinopyroxene, and the observed boundary clinopyroxene may have nucleated and grown from the liquid, along with the larger core clinopyroxene.

INTRODUCTION

There are two fundamentally different classes of Ca-Al-rich inclusions (CAIs): those that partially or completely melted, sometimes more than once; and those (e.g., "fluffy type A") that never melted at all. This divergence in thermal processing implies nebular processes and environments of variable intensity and/or locality, and the objective of much research on these objects is to connect the observed phase assemblages and compositions to the conditions and time scales that produced them. This simple goal is complicated by the fact that many processes, such as volatilization from, and condensation onto, partially molten droplets, crystallization, diffusive relaxation, and low-temperature alteration may all have been important and may have happened more than once. Since observations obtained from any given technique likely bear an imprint from more than one of these processes, the development of new approaches to characterize CAIs and their components is highly desirable. In this study, we use focused ion beam thin section preparation and scanning transmission electron microscopy (FIB/STEM) techniques to obtain a detailed view of the interface between spinel crystals in type B1 CAIs and their host melilites on a much smaller spatial scale than previously attainable. This opens a potential new window into the igneous events that affected these objects and their subsequent evolution.

Type B1 inclusions are classic examples of CAIs that are thought to have passed through a partially molten stage (e.g., Stolper and Paque 1986). The basic igneous mineral assemblage is disarmingly simple: spinel (essentially $MgAl_2O_4$), a binary melilite solid solution (åkermanite [Åk: $Ca_2MgSi_2O_7$]-gehlenite [$Ca_2Al_2SiO_7$]), anorthite (essentially $CaAl_2Si_2O_8$), and a Ti-Al-bearing clinopyroxene, with the bulk inclusion composition encompassed almost entirely within the system CaO-MgO-Al_2O_3-SiO_2-TiOx. Type B1 inclusions are characterized by a melilite-rich, clinopyroxene-poor mantle surrounding a clinopyroxene-rich core that also contains melilite and anorthite. Spinel occurs both in the mantle and core; anorthite, only in the core. Note that these are all crystalline phases. Glass, which is only rarely observed in CAIs, has been attributed to flash melting in rare high-velocity impacts (e.g., Marvin et al. 1970; Stolper 1982); shock-induced oriented amorphous lamellae within melilite have also been reported (Greshake et al. 1998).

Experimental studies focused on type B inclusions have established the order of crystallization, appearance temperatures, liquid lines of descent, major element compositions of solid solutions, and trace element partitioning produced during cooling from high temperatures under various conditions (Beckett et al. 1990; Connolly and Burnett 2003; Lundstrom et al. 2006; MacPherson et al. 1984; Paque et al. 1994; Peters et al. 1995; Stolper 1982; Stolper and Paque 1986), and several recent studies have emphasized the role of volatilization (Mendybaev et al. 2006; Richter 2004; Richter et al. 2002; Richter et al. 2006). These works have yielded useful constraints on the temperature, redox conditions, pressure of the ambient vapor, and time scales for melting, but a common thread is the use of bulk compositions, liquids whose presence and compositions are inferred, not observed, and/or coarse-grained crystals of one or more of the four major crystalline phases. With the exception of opaque assemblages, or Fremdlinge (Armstrong et al. 1985; Blum et al. 1989a, 1989b; Campbell et al. 2003; El Goresy et al. 1978; Palme et al. 1994), and the unusual silicate "UNK" (Barber et al. 1994; Paque et al. 1994), the possible utilization of minor or very fine-grained phases in type B inclusions to infer igneous conditions of formation has been largely neglected. There are good reasons for this. Minor phases often form extremely fine-grained, multi-phase assemblages that are very difficult to characterize using standard scanning electron microscopy (SEM) or electron probe microanalysis (EPMA) techniques. For example, thin rinds and blebs of clinopyroxene are commonly found along grain boundaries of spinel (MacPherson et al. 1984; Kuehner et al. 1989; Simon et al. 1991). Paque et al. (2007a) noted these boundary clinopyroxenes in TS-34, a type B1 inclusion from Allende that is also part of this study, but they were unable to undertake a detailed characterization because of the fine grain size. Similarly, Connolly and Burnett (1999) observed thin "halos" of undetermined mineralogical nature around spinel in anorthite from Leoville 3537-2, the other inclusion we studied, and in TS-23, another Allende type B1 inclusion. These halos were also too thin to evaluate using the techniques available to the authors. Thus, the potential archive of information contained within these grains, which may well be even greater than for the more commonly studied coarse-grained major phases, cannot be fully realized using standard SEM- and EPMA-based analytical and imaging techniques.

In this study, we use SEM and EPMA to provide a basic petrographic context at the scale of a few μm and larger but then use FIB/STEM to characterize small-scale features, a few μm to a few nm across, with an emphasis on the interfacial region between spinels and their host melilites in two type B1 CAIs. FIB/STEM is well posed for imaging and phase characterization of features a few microns across or less (Giannuzzi and Stevie 1999; Heaney et al. 2001; Overwijk et al. 1993), and the technique is advantageous in allowing the observation of specific sites in an object already characterized for mineralogy, petrology and/or isotopic compositions by other analytical techniques (e.g., Bradley et al. 2005; Floss et al. 2004). Thus, mineralogical and chemical studies can be conducted at the nm to μm scale (e.g., identity and semi-quantitative chemical compositions of individual sub-μm minerals and crystallographic relationships between adjacent minerals) to potentially constrain the nature of crystallization and alteration in CAIs. Phase identification was made by electron diffraction, X-ray spectra, and electron energy loss spectra (EELS).

There is a relatively extensive literature on the TEM characterization of presolar grains in meteorites (e.g., Bernatowicz et al. 1991; Croat et al. 2005; Daulton et al. 2002, 2003; Nguyen et al. 2007; Stroud et al. 2004). Previous applications of TEM techniques to Allende and Leoville CAIs (e.g., Barber et al. 1984; Keller and Buseck 1991, 1994; Müller 1978; Müller and Wlotzka 1982), however, mostly involved the use of Ar ion milling, which is not capable of targeting specific small-scale features. These CAI studies have nevertheless led to important constraints on the shock histories of the inclusions, insights into defect and dislocation densities of the constituent phases, and to the conclusion that hydrated phases, while quite rare, do occur in Allende CAIs. FIB/STEM has been used to study SNC meteorites (Bleiner et al. 2006; Heaney et al. 2001), the terrestrial alteration of ordinary chondrites (Lee et al. 2003) and, more recently, CAIs (Ford and Brearley 2007; Paque et al. 2007c; Toppani et al. 2006). In this study, we emphasize the application of FIB/STEM techniques to boundary clinopyroxenes, blebs and rinds of clinopyroxene found on spinel grains included in melilite from type B1 inclusions, and to associated phases. Preliminary accounts of this work were presented by Paque et al. (2007b; 2007c).

EXPERIMENTAL AND ANALYTICAL TECHNIQUES

Analytical Techniques

Initial characterization of meteoritic samples was performed using the LEO 1550 VP field emission scanning electron microscope and the JEOL 733 and JEOL JXA 8200 electron microprobes at Caltech. The experimental run product was analyzed using the JEOL 733. Analytical conditions for the electron probe included an accelerating voltage of 15 kV, a beam current of 20 to 40 nA, and a beam diameter of ~1 μm. Synthetic and natural minerals were used as standards and data reduction was done through a CITZAF correction procedure (Armstrong 1988). Detection limits for most analyses were 0.01 to 0.02 wt%, with typical one sigma counting statistics errors of less than 0.5% for major elements, increasing with decreasing concentration. Unless otherwise stated, all errors quoted in this work refer to one standard deviation of the mean. Electron-transparent thin sections of spinel-melilite interface regions were prepared at Lawrence Livermore National Laboratory (LLNL) using an FEI Nova NanoLab 600 dual-beam focused ion beam instrument (FIB). The FIB has an electron and an ion column (30 kV Ga^+) with Pt and C deposition capabilities, in-chamber manipulators for in situ section liftout and an EDAX energy dispersive spectrometer. STEM analysis was performed at LLNL using a 200 kV FEI Tecnai20 G2 monochromated (S)TEM, equipped with a high angle annular dark field detector, Gatan high-resolution imaging filter, and EDAX Si(Li) energy-dispersive spectrometer. EELS were acquired at the O-K edge with 5.6 mrad collection angle and 0.05 eV/channel dispersion. The energy loss was calibrated by the zero loss peak after each spectra. Due to sample sensitivity to beam damage, a low-intensity beam was applied to the measurement regions for long (several minute) acquisition times. EELS energy resolution is on the order of 1 eV.

Experimental Techniques

We conducted a dynamic crystallization experiment on a melilite-rich CAI-like bulk composition (“98”) using techniques described in Stolper and Paque (1986). The bulk composition, which is most relevant to type A inclusions and the mantles of type B1s, and a summary of additional isothermal and dynamic crystallization experiments on this bulk composition are given by Paque and Stolper (1984). Briefly, a slurry of powdered glass starting material in polyvinyl alcohol was placed on a Pt loop, air dried, and then suspended in air in a Deltech DT-31 vertical gas mixing furnace. The sample was held at an initial temperature of 1500 °C for 3 hours, cooled at 2 °C/h to 1167 °C and drop quenched into deionized water. The run product was polished as a thin section and characterized using the SEM and electron microprobe.

Meteoritic Samples and FIB Procedures

We studied two type B1 inclusions. Allende TS-34 is a large, spherical inclusion ~9 mm in diameter showing only a moderate degree of secondary alteration, which has been the subject of numerous studies (e.g., Beckett et al. 2000; Clayton et al. 1977; Connolly et al. 2003; Paque et al. 2007a; Simon et al. 1991). Leoville USNM 3537-2 is a coarse-grained spherical type B1 CAI ~7 mm in diameter (Caillet et al. 1993; Connolly and Burnett 1999). Both inclusions are interpreted to be igneous objects that partially or completely melted and cooled under reducing conditions.

In the course of studying minor element concentrations in TS-34 spinels, Paque et al. (2007a) noted the common occurrence of clinopyroxene on spinel inclusions in melilite. These grains were generally too thin to fully characterize and, therefore, the interface regions between spinel and melilite in five areas were chosen for more detailed FIB/STEM examination. Three of these grains, A2, E2 (mantle) and B2 (core) from TS-34, were previously studied by Paque et al. (2007a). Two additional spinel grains, one each from the mantle (Leo1) and core (Leo2), were selected from Leoville 3537-2 based on SEM examination.

Electron-transparent sections of the interface region between spinel and melilite were prepared using the FIB at LLNL. The chosen location was first protected from amorphization and ion implantation by chemical vapor deposition of a 2–3 μm thick, ~15 to 20 μm long Pt-strap through interaction of a locally injected organometallic gas with the electron or ion beam. This was followed by ion beam milling of trenches on both sides and channels at the edges to produce an ~1–2 μm thick section (Giannuzzi et al. 1998; Giannuzzi and Stevie 1999; Heaney et al. 2001; Overwijk et al. 1993) nearly free from the surrounding material and connected only at one corner. This preliminary section was extracted at greater thickness than most examples cited in the literature to further reduce the concentrations of implanted Ga and redeposited material in the final thinned section. The thick section was extracted from the bulk material by “welding” it using Pt deposition to a tungsten needle controlled by micromanipulator and severing the final connection to the surrounding material using the ion beam. In a similar fashion, the section was “welded” to a specially designed TEM grid and the connection to the tungsten needle severed. Sections were ion beam thinned in situ to ~100 nm for electron beam transparency. Although the precise thickness of surface structural damage caused by the sample preparation is sensitive to both the material and ion milling parameters (Giannuzzi and Stevie 1999; Prenitzer et al. 2003), extremely fragile samples such as clays, phyllosilicates, and even organic material can be studied using the FIB procedures of this study (Lee et al. 2003; Obst et al. 2005).

RESULTS

Experimental Results

The run product for dynamic crystallization experiment 98-53 produced euhedral melilite enclosing spinel. In some cases, spinel plus liquid was trapped in the growing melilite crystal (Fig. 1a), from which clinopyroxene crystallized at lower temperatures along with a more magnesian (i.e., higher Åk) melilite on the walls of the melt inclusion.

Glass compositions are homogeneous but the adjacent melilite can be strongly zoned. The lower panel of Fig. 1b shows an example of melilite compositions in dynamic crystallization experiment 98-53 as a function of distance from the interface with glass. A total of seven such profiles approaching melilite-glass or clinopyroxene-glass interfaces were obtained. All of the melilite is zoned, but as some interfaces with glass are approached, the melilite becomes unusually åkermanitic (magnesian). Åk contents of the melilite along one traverse shown in Fig. 1b increase by ~30 mole% within 10 μm of the interface. Based on regional variations in melilite composition, negligible variations in Åk would be expected. Similarly, melilite at some, but not all, clinopyroxene-melilite contacts show Åk enrichments. We have observed similar behavior for other unpublished experiments conducted over a broad range of liquid compositions and run conditions. Not every direction extending from glass-melilite contacts will show these anomalous increases in Åk, but some invariably do. Thus, the expectation based on experiment is that liquids trapped in melilite will continue to fractionate, yielding additional åkermanitic melilite near the interface with glass or clinopyroxene. It is also important to note that, due to differences in the direction of crystallization of the melt inclusion relative to the plane of the polished section, glass-melilite or clinopyroxene-melilite boundaries without such Åk enrichments are also observed. Hence, multiple determinations of near-interface melilite compositions are required to establish whether or not a particular clinopyroxene is or is not associated with anomalous zoning of the adjacent melilite.

SEM Petrography of Meteoritic CAIs

Figure 2 is a pair of backscattered electron (BSE) photomicrographs showing well developed examples of boundary clinopyroxene on melilite-hosted spinels from the mantle and core regions of Allende type B1 inclusion TS-34, similar to those previously seen by MacPherson et al. (1984), Kuehner et al. (1989), and Simon et al. (1991). Clinopyroxene occurs both as a continuous or nearly continuous rim or "rind" up to ~5 μm thick, extending over tens of μm along a crystal edge (Fig. 2a) and as discontinuous blebs less than 1 to as much as 8 μm in maximum thickness (typically 1–3 μm thick;

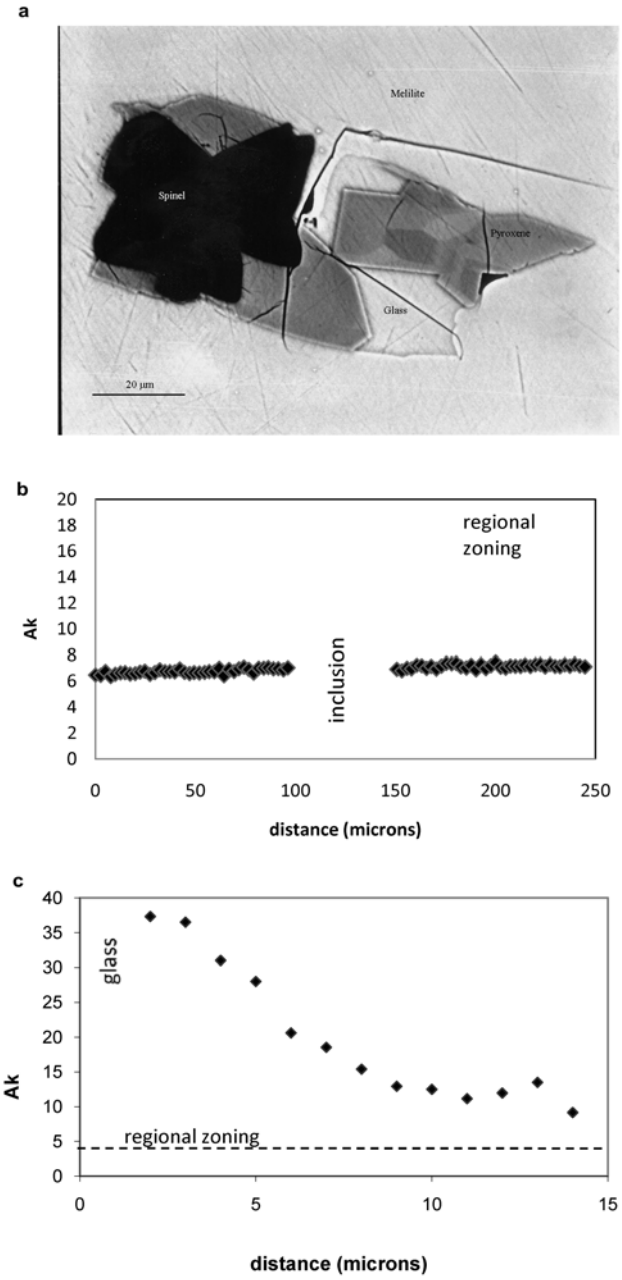

Fig. 1. Run product from dynamic crystallization experiment 98-53 (conducted in air, initially at 1500 °C for 3 h followed by cooling at 2 °C/h to 1167 °C). a) Backscattered electron photomicrograph of a spinel-clinopyroxene-glass inclusion in melilite. Scale bar is 20 μm. The arrow indicates the location of the traverse in Fig. 1b. b) Mole% åkermanite (Åk) in melilite as a function of distance to an interface with the inclusion. The upper panel shows the regional pattern of zoning in the melilite in the general vicinity of the spinel inclusion. There is a slight (~2 mole%) decrease in Åk over a distance of 250 μm. The lower panel shows zoning in the immediate vicinity of the inclusion. There is a ~30 mole% increase in Åk in the 10 μm closest to the glass adjacent to the spinel.

Fig. 2b). The melilite in TS-34, like other Allende CAIs, is variably altered to fine-grained mixtures of grossular,

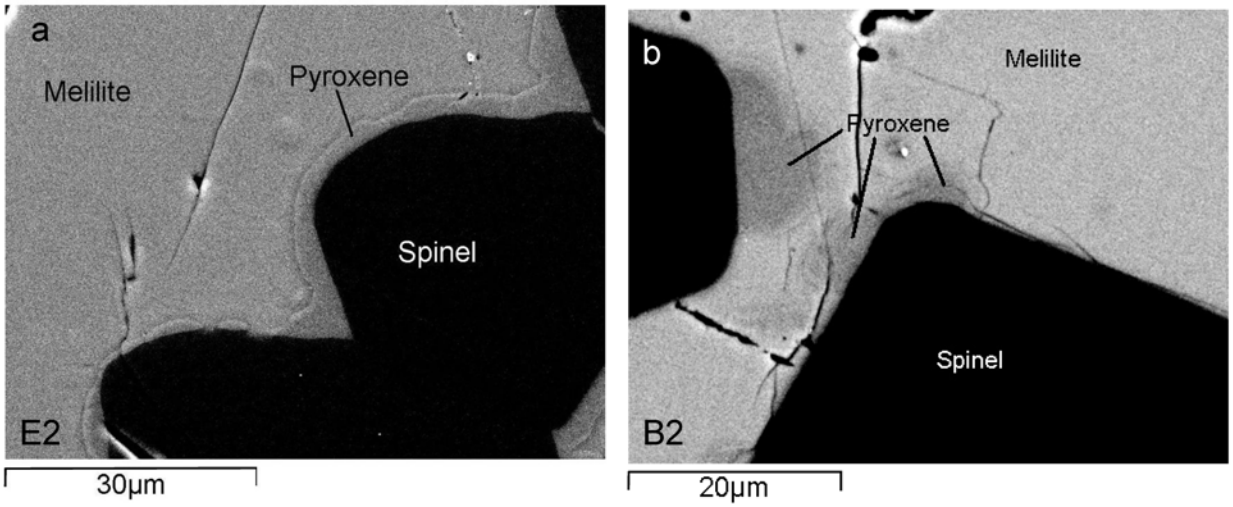

Fig. 2. Backscattered electron photomicrographs of examples of boundary clinopyroxene from Allende TS-34. a) Clinopyroxene rind decorating a cluster of spinel crystals in the mantle. A larger scale view of this area is given in Fig. 4b (grain E2) of Paque et al. (2007a). b) Clinopyroxene blebs on spinel in core melilite (grain B2 of Paque et al. [2007a]).

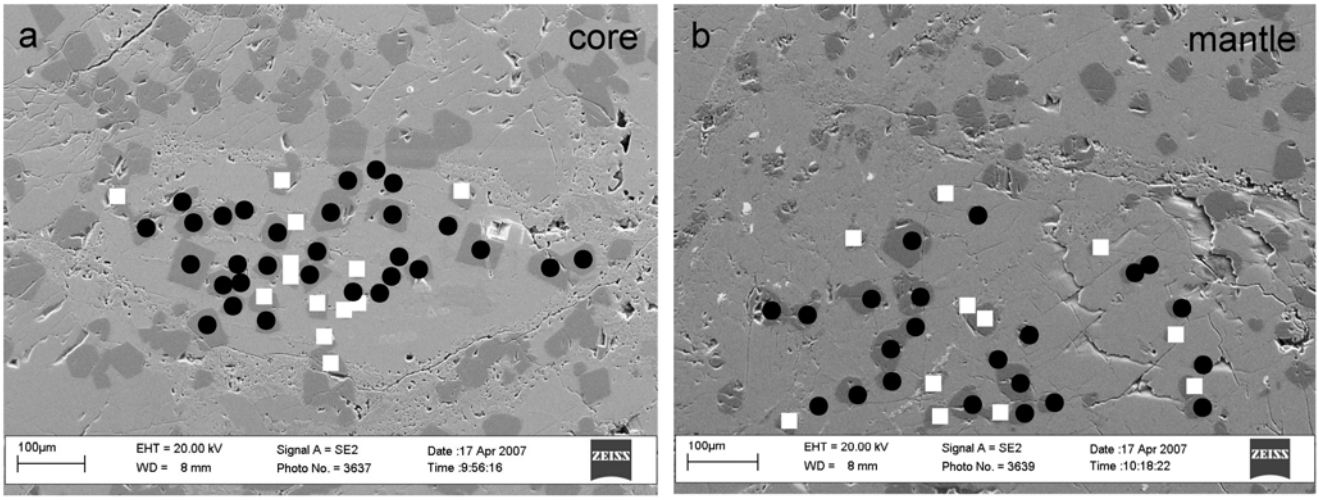

Fig. 3. Backscattered electron photomicrographs of Allende TS-34 spinels included in (a) core and (b) mantle melilite. Spinel grains decorated by boundary clinopyroxenes are indicated by black circles and those lacking boundary clinopyroxenes by white squares. Scale bars are 100 μm.

monticellite, and wollastonite (Davis et al. 1994) but there is no correlation between the presence or absence of boundary clinopyroxene and areas of alteration in TS-34.

Close examination of the interfacial region between spinel and melilite in TS-34 shows that ten of the eleven TS-34 spinel grains and clusters studied by Paque et al. (2007a) have boundary clinopyroxenes. Of the eight spinels in mantle melilites they analyzed, six have clinopyroxene rinds, one is associated with blebs, and one has both a rind and blebs. No core spinels in melilite were found to have clinopyroxene rinds but two of three have associated blebs. Thus, spinels in this population of grains that are free of boundary clinopyroxene in the plane of the section appear to be rare, and allowing that some sections through spinel crystals with blebs may miss all of them, it is possible that all eleven spinel occurrences described by Paque et al. (2007a) have boundary clinopyroxene.

Since Paque et al. (2007a) selected relatively large grains for minor element mapping, we also made a systematic survey of small spinels from an ~300 × 700 μm, relatively spinel-rich melilite from the core of TS-34 (Fig. 3a) and from a similarly sized portion of a melilite crystal from the mantle (Fig. 3b). All of the spinel grains in the mantle test area that lack boundary clinopyroxenes are relatively small, but overall, most of the small spinels have boundary clinopyroxenes, suggesting that the presence of blebs or rinds is endemic among spinel grains of all sizes. In an area of similar size in the core (Fig. 3a), spinel grains lacking

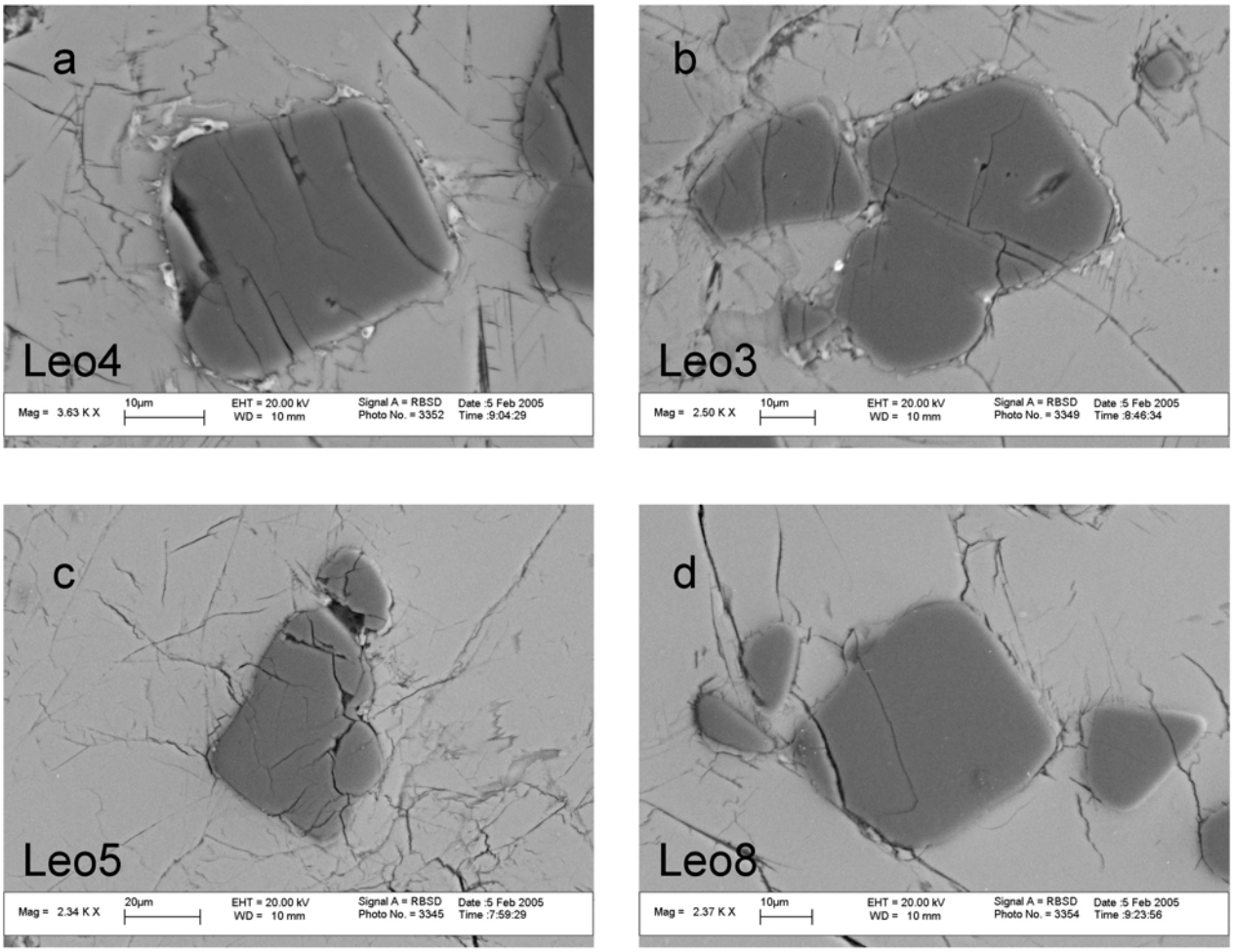

Fig. 4. Backscattered electron photomicrographs of spinels in host melilite from Leoville 3537-2. a) Leo4; scale bar 10 µm. b) Leo3; scale bar 10 µm. c) Leo5; scale bar 20 µm. d) Leo8; scale bar 10 µm.

boundary clinopyroxenes lie mostly along a central swath through the test area; there may be two populations of spinels, not size related, one of which lacks boundary clinopyroxenes. Based on semi-quantitative EDS analyses, Ti contents of the cores of spinel grains shown in Fig. 3a are similar for both populations and are typical of those of core spinels. Thus, the presence or absence of boundary clinopyroxenes is not correlated with the spinel composition. Moreover, since compositions of mantle and core spinels are distinct from each other (Connolly et al. 2003; Paque et al. 2005), we know that the boundary clinopyroxene-free cluster in Fig. 3a is not a group of spinel grains originally located in the inclusion mantle that was later transported into the core.

Leoville 3537-2 spinels also have boundary clinopyroxenes but the textural relationships are more complex than in TS-34, even at the SEM level. Figure 4 shows BSE photomicrographs of spinel grains included in melilite from Leoville 3537-2. Each has one or more phases present on the grain boundary between spinel and melilite. As with TS-34, both continuous (rinds) and discontinuous (blebs) boundary phases are observed. Clinopyroxene is evidently among the phases present based on semi-quantitative analyses, but it was not possible through SEM examination to establish the identity of other phases except the calcite observed filling fractures in melilite near one of the spinel grains, Leo1, that we consider in detail below. Since Leoville 3537-2 is a nominally unaltered inclusion, the complexity is not simply a consequence of differences in alteration processes for the two inclusions, although we revisit this inference below.

In both TS-34 and 3537-2, boundary clinopyroxenes are generally too narrow for quantitative electron microprobe analysis, but EDS analysis of relatively thick examples demonstrates that the boundary clinopyroxene compositions are similar to those of coarse-grained mantle clinopyroxenes (i.e., high in Ti and Al) in TS-34 analyzed by Simon et al. (1991), Simon and Grossman (2006), and in this study. Results also show that boundary clinopyroxenes on core spinels are typical of core clinopyroxene (i.e., lower in Ti and Al). We also analyzed a relatively coarse-grained, isolated (in

the plane of the section) mantle clinopyroxene and found, as have others (Lin et al. 2003; Simon et al. 1991), that Sc concentrations are often fairly high (up to 0.3 wt% Sc_2O_3). Scandium zoning is somewhat patchy but the lowest concentrations (<0.15 wt%) are restricted to outer portions of the crystal.

While the boundary clinopyroxenes are generally thin and difficult to analyze using SEM/EPMA techniques, melilite compositions around the spinel grains are readily analyzed, although spatial resolution is poor within ~5 μm of the interface. Figure 1b shows that crystallization of melilite from a melt inclusion results in large Åk gradients decreasing away from some, but not all, clinopyroxene or glass interfaces. Thus, any search for Åk gradients in natural CAIs adjacent to boundary clinopyroxene ascribable to melt inclusions must have a good statistical basis. Primarily using 2-dimensional melilite composition maps (2–8 μm step size) centered on mantle spinel grains with observed boundary clinopyroxene, we extracted those analyses which define Åk profiles approximately normal to melilite—boundary clinopyroxene or melilite—spinel interfaces. Melilite compositional variations adjacent to the boundary were observed in 33 profiles near four spinel grains, but these were relatively small (change in Åk less than 6 mole%) and some of this could be due to secondary fluorescence of Mg from the spinel. For melilite in the region around spinel grain A2, Åk oscillations between Åk22 and Åk25 are observed at distances that are large compared to the thickness of the boundary clinopyroxene, with occasional "hot spot" excursions to Åk30–36. It is probably inevitable that, whatever the origin of the boundary clinopyroxene, there will be some accompanying perturbation in the composition of the adjacent melilite. It is likely significant that Åk variations around boundary clinopyroxene in TS-34 are much smaller than those observed from the crystallization of the synthetic melt inclusion (Fig. 1b). The issue of Åk gradients near spinel-melilite interfaces is also addressed below based on a higher spatial resolution examination of the FIB section composition profiles.

In summary, based on SEM/EPMA results, boundary phases on spinel-melilite interfaces are quite common in both Allende TS-34 and Leoville 3537-2. These boundaries appear to be dominated by clinopyroxene in TS-34 but may involve additional phases in 3537-2.

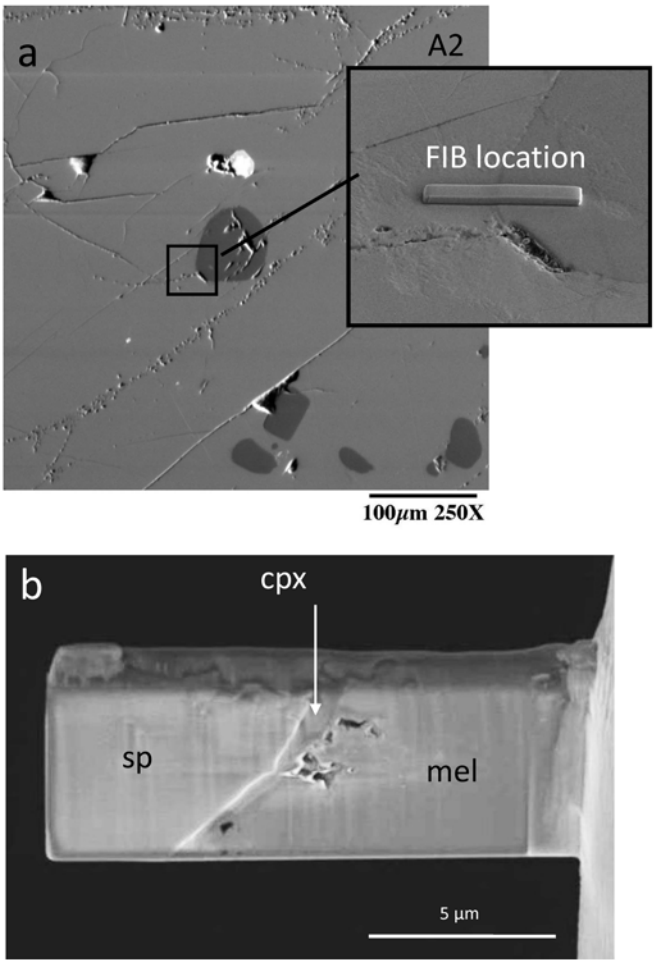

Fig. 5. a) Backscattered electron photomicrographs of Allende TS-34 mantle spinel grain A2, centered in the image, with an inset detailing the location of the FIB/STEM cross section sample (at a tilt angle of 52° after deposition of a protective Pt strap but prior to FIB trench milling). The bright object above spinel grain A2 in the main panel is an opaque assemblage. Scale bar for the main panel is 100 μm. (b) SEM images of a FIB-thinned section of the interface between spinel and melilite for Allende TS-34 spinel grain A2 obtained in the FIB on a FIB section. The section is mounted on a TEM grid (right) by a ~1 μm thick layer of Pt and protected from ion implantation by a Pt layer (top). A nearly continuous layer of 0.2–0.8 μm thick clinopyroxene resides between the melilite and spinel. Toward the bottom of the section, a cluster of small pyroxene crystals lie on the melilite side of the boundary. Dark spots are voids. Scale bar is 5 μm. Abbreviations are sp (spinel), cpx (clinopyroxene), and mel (melilite).

FIB/STEM Studies

Based on SEM imaging, five spinel grain interfaces were selected for FIB/STEM analysis. Figure 5a shows one of these, spinel grain A2 from the mantle of TS-34, along with the location of the FIB section eventually removed (marked by a protective Pt strap). We selected A2 and the specific location of the section to study a thin clinopyroxene rim between the spinel and melilite, the presence of which was inferred based on Ti hot spots in the Ti maps obtained by Paque et al. (2007a) but not well resolved by SEM imaging. SEM-EDS analyses of melilite in the region around the trench show Åk20 to Åk25, typical of values in other areas of melilite adjacent to A2. An SEM image of this boundary in the FIB section prior to final thinning (Figure 5b) confirms clinopyroxene with no other phases present. On a submicron scale, the clinopyroxene rim adjacent to the spinel surface consists of clinopyroxene crystals that vary in thickness, one

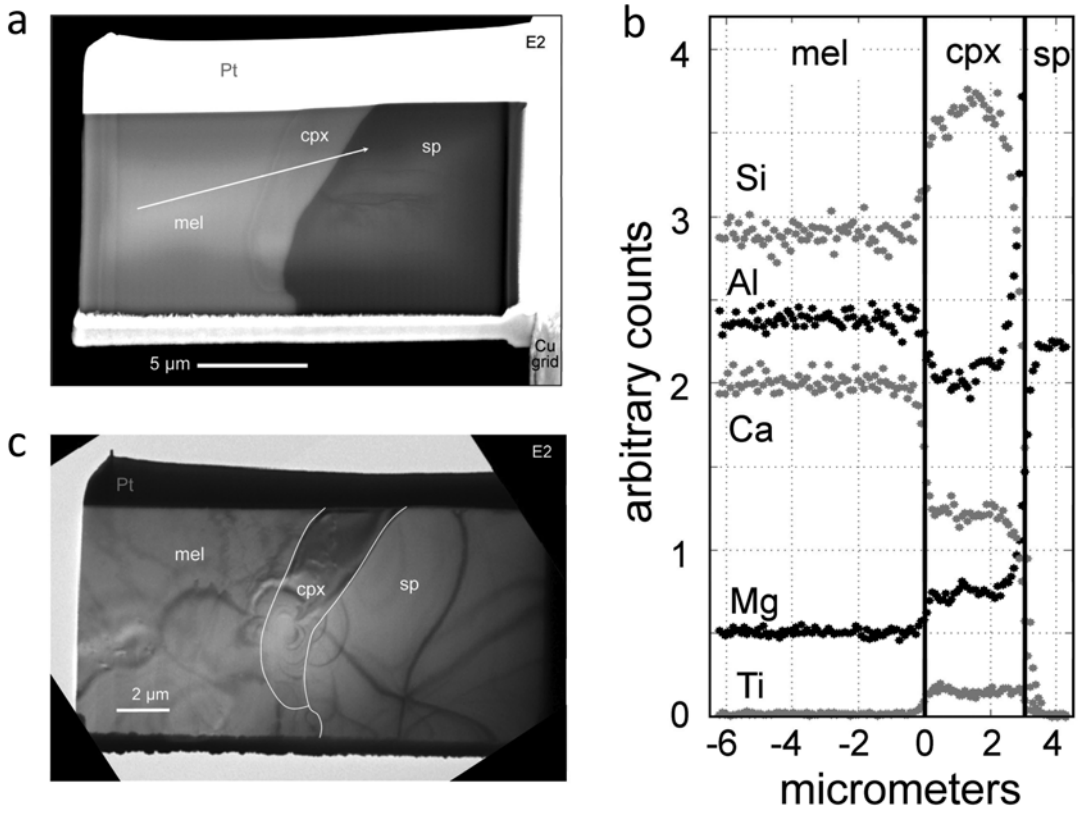

Fig. 6. Mantle spinel grain E2. a and b) Backscattered electron photomicrograph with the location of the traverse indicated, and the corresponding EDS linescan. c) Low magnification brightfield TEM image of interface region between spinel and melilite.

portion ~0.1–0.2 µm thick and a second, considerably thicker region, ~0.7 µm. Near the base of the section and near the junction between the two large clinopyroxenes, there appear to be clusters of small crystals that extend into the melilite. Thus, the spinel side of the contact is relatively smooth and the melilite side more irregular, although the clinopyroxene-melilite interface appears smooth at any particular point. Unfortunately, the FIB section for A2 did not survive final thinning to electron-transparency for TEM analyses and we were therefore unable to further characterize it.

FIB/STEM section E2 was taken across a spinel-melilite interface in the mantle of TS-34. An SEM image of the section is shown in Fig. 6a and a traverse across the interface is shown in Fig. 6b. There is no significant variation in the melilite chemistry, which contrasts with the synthetic sample (Fig. 1b). Note that SEM-EDS spatial resolution is considerably higher in Fig. 6b than can be obtained on a standard thin section because the present sample is only 1.5 µm thick. Since the analyzed sample is so thin, the interaction volume is smaller than in a thick sample and, therefore, loss of spatial resolution due to the electron interaction volume is significantly reduced. The interface profiles in Fig. 6b are also sharp (e.g., Ca), consistent with the roughly 0.8 µm diameter electron beam. Figure 6c shows a low-magnification, conventional brightfield TEM image of the interface region. Clinopyroxene-spinel and clinopyroxene-melilite interfaces are sharp with no additional phases present, but high-resolution examination reveals that melilite and spinel are separated by an ~150 nm thick boundary phase. This may be a secondary mineral (not clinopyroxene) but we have not established its identity.

FIB section B2-1 was made at a location on core spinel grain B2 that showed no Ti hot spots in the Ti map obtained by Paque et al. (2007a), and no boundary clinopyroxene during SEM examination (Fig. 7a). This location was selected to see if an FIB/STEM section of a melilite-spinel boundary showing no boundary clinopyroxene at the µm scale was also devoid of clinopyroxene at the nm scale. This issue is important because clinopyroxene or some other phase always separating spinel from melilite would hint at a reaction between melilite or liquid and spinel, or some universal process by which clinopyroxene invariably forms on spinel and is never subjected to a process that could remove an extremely thin layer. The FIB/STEM section, however, shows a clean, sharp interface between the spinel and melilite. It is clear from Allende spinel grain A2 (Fig. 5b) that the thickness of clinopyroxene rinds can vary significantly but extremely thin layers of clinopyroxene <~0.1 µm are not observed. Section B2-1 demonstrates that direct contact of spinel with melilite does occur even at the scale of a few nm and that clinopyroxene-decorated spinel surfaces, although extremely common, are not universal.

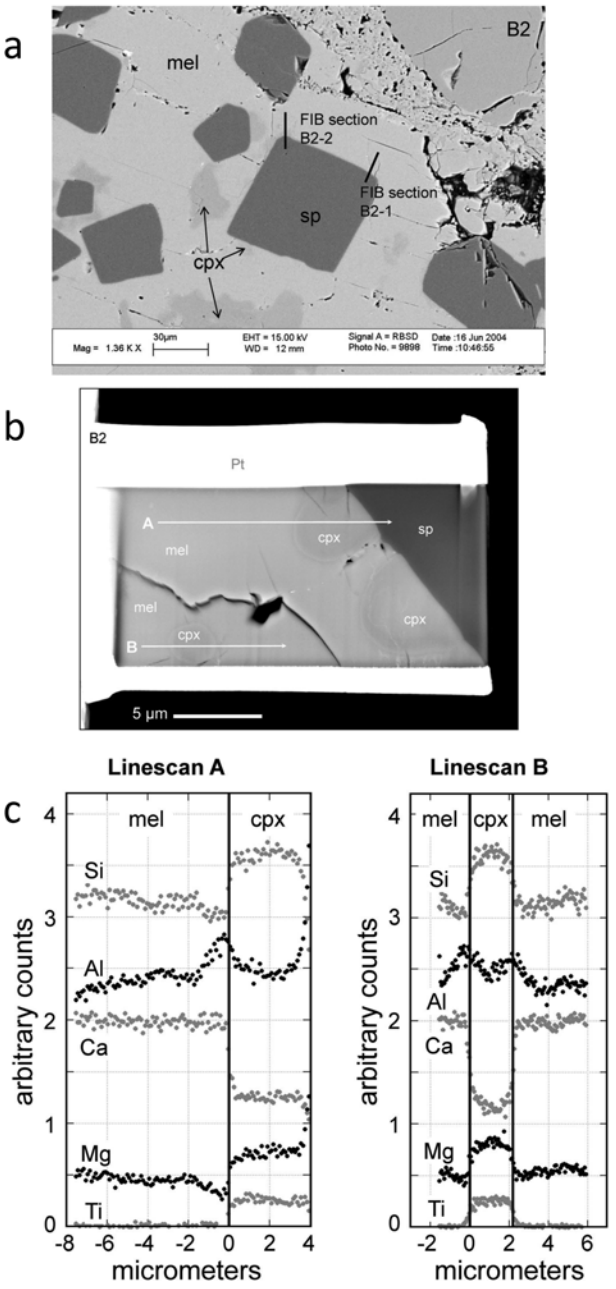

Fig. 7. Isolated (in the plane of the section) and boundary clinopyroxene in FIB section B2-2 of core spinel grain "B2" from Allende TS-34. a) Backscattered electron photomicrograph of spinel grain B2 with the location of the FIB sections indicated. FIB section B2-1 was made from a location where clinopyroxene was not observed during SEM examination. b) Backscattered electron photomicrograph of section B2-2 with locations of traverses indicated. c) EDS linescans across the isolated and a boundary clinopyroxene into adjacent melilite are also shown.

A second FIB section was prepared from core spinel grain B2 at a location where boundary clinopyroxene was indicated in the SEM maps. Figure 7b shows the spinel interface regions for the FIB section B2-2. This section is characterized by two blebs of boundary clinopyroxene in

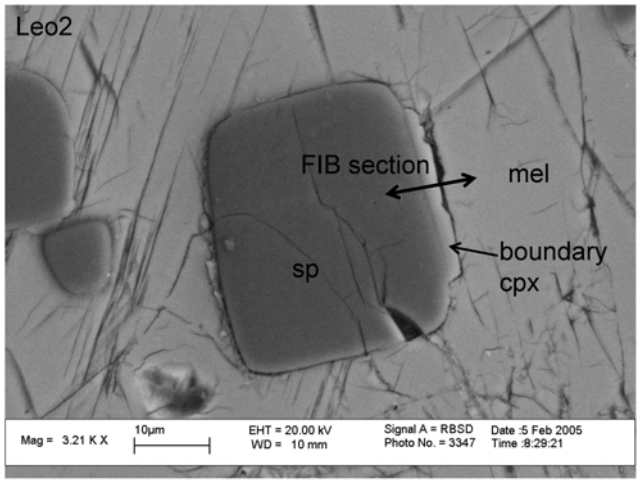

Fig. 8. Backscattered electron photomicrograph of spinel grain Leo2 in core melilite of Leoville 3537-2. The location of the FIB section is indicated by the double-headed arrow. Scale bar is 10 µm.

contact with spinel and a third, similarly sized, apparently isolated, clinopyroxene grain ~10 µm away. The host melilite for B2 is ~Åk50, typical of core melilite in TS-34. Four SEM line scans (~0.8 µm beam width) were obtained on the FIB section, two of which are shown in Fig. 7c. Data for the other two line scans are similar. Because these data were obtained from a sample 1.5 µm thick, the SEM spatial resolution is higher than would be obtained on a traditional, ~30 µm (effectively infinitely thick) section. All three clinopyroxenes are rimmed with melilite ~2 µm thick that becomes more åkermanitic with distance away from the clinopyroxene-melilite interface until it matches the composition of the host melilite. The linescans are semi-quantitative but, based on spot analyses in or near the traverses, the range in Åk in Fig. 7c is a few mole% and the average near the clinopyroxene-melilite interfaces is ~Åk45. Note that the Åk gradients are in the opposite sense and much smaller in magnitude than those observed near the experimental melt inclusion (Fig. 1b).

Two spinel grains from Leoville 3537-2 were selected for FIB/STEM study. Spinel grain Leo2, from the core of the inclusion, is shown in Fig. 8 along with the location of the FIB section. This section crosses an unusually thick boundary clinopyroxene that lies along one side of the spinel grain in the SEM photomicrograph. An electron microprobe measurement of the melilite composition in the vicinity of the FIB section gives Åk51, typical of core melilites in this inclusion. Figure 9, a brightfield TEM photomicrograph, provides an overview of the interface region, and higher magnification images are shown in Figs. 10–12. A clinopyroxene rim of variable thickness from 0.5 to 2 µm is in contact with the spinel, with a smooth interface between them (Fig. 9). Multiple spinel crystals are evident in the FIB section intersecting spinel grain Leo2. Polycrystalline spinel was not observed in any of the other FIB sections although this could

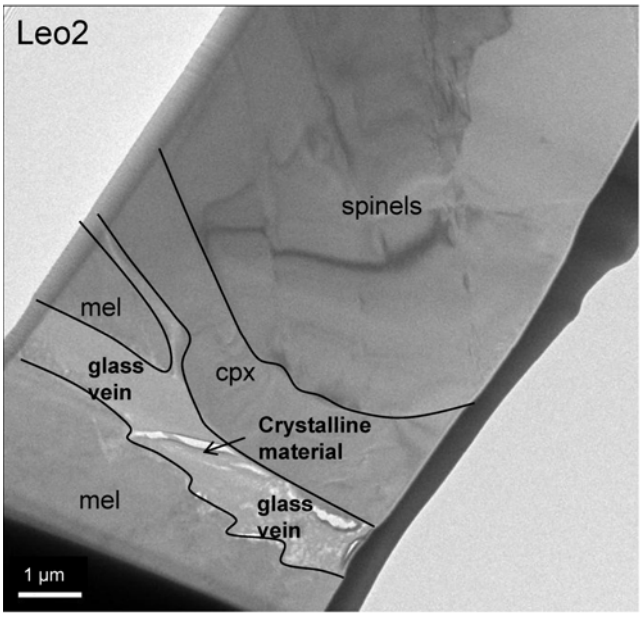

Fig. 9. Low magnification brightfield TEM image of the interface region between spinel and melilite in Leo2 from Leoville 3537-2. Melilite is separated from spinel by both clinopyroxene and glass. The elongated white regions in the glass vein are cracks. A crystalline phase lines the longest crack. Scale bar is 1 μm.

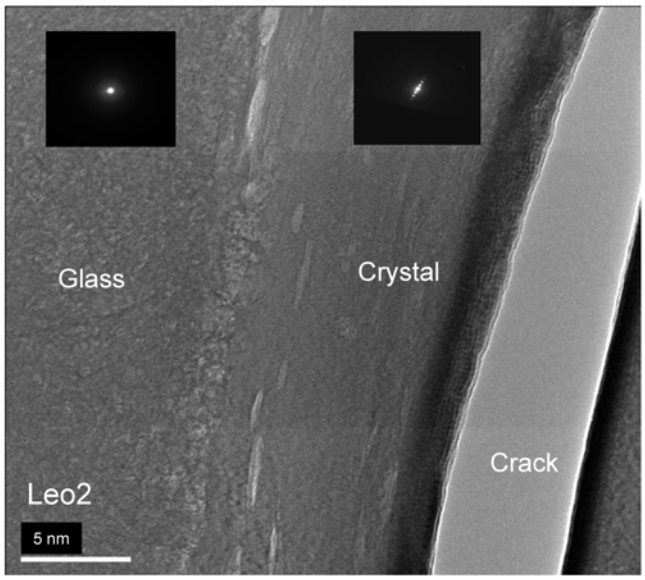

Fig. 10. High magnification brightfield TEM image of the interface between glass and unidentified crystal in spinel Leo2 from Leoville 3537-2, with electron diffraction patterns for the glass and crystal inset. The dense rim at the edge of the crack is most likely caused by redeposition during ion milling. Scale bar is 5 nm.

reflect smaller portions of excavated spinel. Unlike TS-34 spinels, the boundary clinopyroxene on spinel is not in direct contact with the host melilite, being separated by a vein of mostly glassy material, generally ~1 μm across, showing electron diffraction typical of amorphous phases. Where this glassy layer is in contact with clinopyroxene, the interface is smooth, but melilite-glass interfaces are rough, typical of corrosion (Fig. 11a), with apparent intrusion into the melilite along cracks or cleavage traces. This is true both of the melilite "peninsula," a portion of which can be seen in Fig. 9, and the host melilite. A typical glass composition is 25 wt% MgO, 20% Al_2O_3, 47% SiO_2, and 8% CaO with < 1 wt% FeO, TiO_2, or Na_2O, a composition which is Mg-, Si-rich and Ca-poor relative to the coarse-grained igneous silicates.

In the central portion of the glassy layer in Fig. 9, there is an unidentified Mg-, Al-rich, Ca-, Si-poor crystalline material. This phase crosses the glass vein and is in contact with clinopyroxene elsewhere in the section (Fig. 11b). Based on electron diffraction patterns (e.g., Fig. 10 inset) and high-resolution imaging, this is a single-phase mineral with a layered lattice structure. Further characterization would require additional material due to the vulnerability of this mineral to electron-beam damage.

Figure 12 shows a low-magnification conventional brightfield TEM image of the glass vein with unidentified crystals and surrounding mineral phases. The locations of oxygen electron energy loss spectra (EELS) for regions containing glass only, crystals plus some glass, clinopyroxene and spinel are indicated. Both the glass and unidentified crystals are electron beam sensitive and it was therefore necessary to obtain the EELS spectra using a broad beam of low intensity. These are shown as insets in the image. A pre-peak is visible about 8 eV below the main peak in the O-K edge absorption spectra from both the glass and unidentified crystals (with included glass) regions. The nominally anhydrous minerals spinel and clinopyroxene show no pre-peak. In hydrated minerals, the pre-peak is indicative of OH-groups, and the ratios of the pre-peak to main peak heights scale with the concentration of OH- (Wirth 1997). The glass-only region shows a pre-peak to main peak height ratio of 0.2, indicative of the presence of OH- and similar to hydroxyl-bearing minerals like talc. The concentration of OH- is, however, indeterminate, as quantitative data of Wirth (1997) refer to crystalline phases, not glass. We are not aware of previous reports of hydrated glasses in CAIs. Wlotzka and Wark (1982), however, reported zeolites in a Leoville CAI, which would be consistent with the presence of hydrated phases, possibly preterrestrial, in 3537-2.

In the unidentified crystal, the pre-peak to main peak ratio for a mixture of ~1/3 glass and ~2/3 crystal is even higher, >0.35 (Fig. 12c), than it is for the glass (~0.2 [Fig. 12d]; i.e., the ratio in the unidentified crystal probably exceeds 0.4). From the data of Wirth (1997), OH- computed as H_2O for this phase exceeds ~20 wt%. The crystals show an elongated, fibrous texture in high magnification imaging and a diffraction pattern typical of layered hydrated mineral phases (Fig. 10). Local composition measurements indicate an Mg-, Al-rich, Ca-, Si-poor phase with Mg/Al > 1.6. Given the very high OH- content of the crystal, its Mg-Al rich

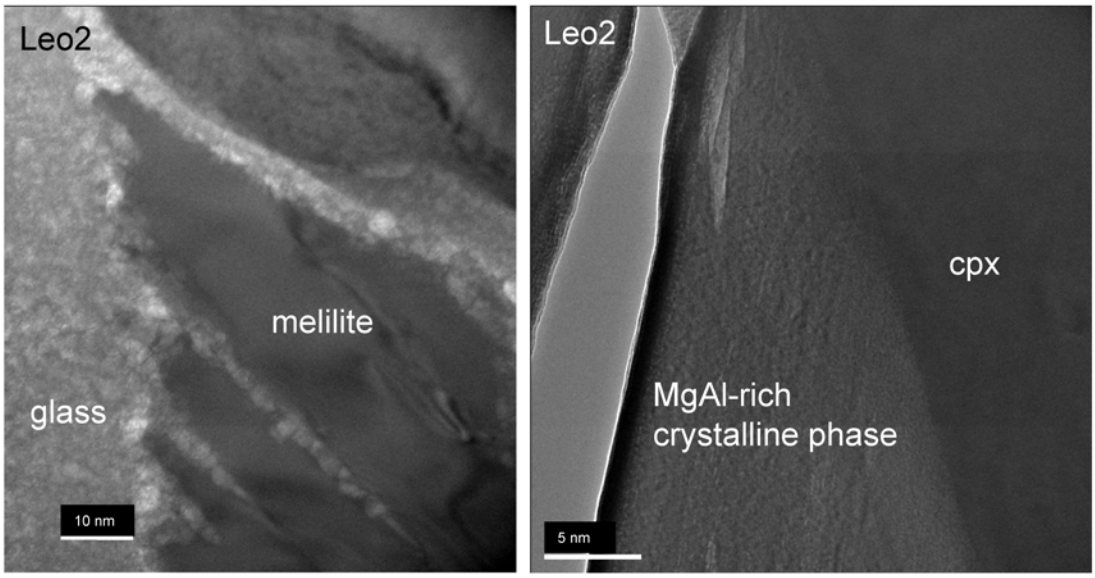

Fig. 11. High magnification brightfield TEM image of interface region between glass and other phases around spinel Leo2 from Leoville 3537-2. a) Glass-melilite interface with melilite surrounded by glass. b) Interface between boundary clinopyroxene and unknown crystal. Scale bars are 10 (left panel) and 5 nm.

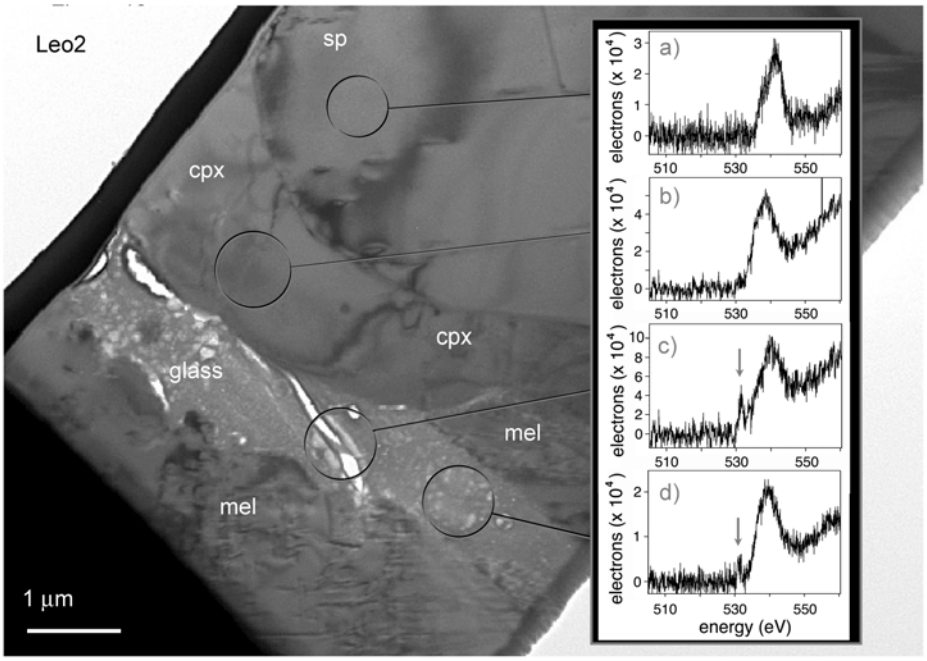

Fig. 12. Brightfield TEM image of the glass vein containing unidentified crystals and surrounding phases that border the core spinel Leo2 from Leoville 3537-2. Inset are oxygen K absorption edge electron energy loss spectra (EELS) from indicated regions containing a) spinel, b) clinopyroxene, c) the unidentified crystal phase plus some of the surrounding glass (approximately 30% by area), and d) glass in the vein. A pre-peak indicative of OH-groups in hydrated phases (Wirth, 1997), indicated by arrows, is visible about 8 eV below the main peak in the O edge of spectra for the unidentified crystal and glass (c, d) but not in clinopyroxene or spinel (a, b).

composition, high Mg/Al ratio, and layered structure, we speculate that this is a layered double hydroxide (Rives 2001) with Mg/Al ~ 2, similar to meixnerite but with a lower Mg/Al.

The Leoville 3537-2 mantle spinel Leo1 (Fig. 13) is superficially similar to other Leoville spinels, like those shown in Figs. 4 and 8, in having a thin, discontinuous rim of clinopyroxene and other phases on the surface of the grain. Leo1 was selected for FIB/STEM because there are also several veins in melilite in the vicinity of the spinel whose mineralogical characteristics could not be established

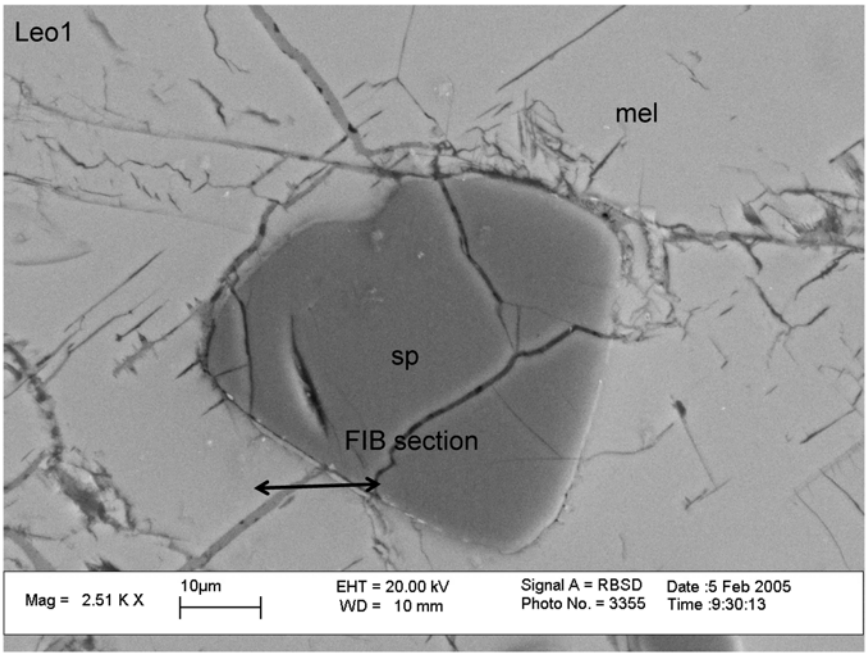

Fig. 13. Backscattered electron photomicrograph of mantle spinel Leo1 from Leoville 3537-2. The location of the FIB section is indicated by a double-arrowed line segment. Scale bar is 10 µm.

unequivocally through SEM examination, although compositions were consistent with calcite as the predominant phase. These veins inhabit cracks in melilite that reach, but do not crosscut, the spinel. In contrast to other FIB sections, which were oriented perpendicular to the spinel surface, the FIB section for Leo1 was deliberately oriented at a lower angle in order to simultaneously sample both the spinel/melilite interface and a section of vein in the host melilite. Figure 13 shows the location of the extracted FIB section. The vein in the host melilite, which is shown in a darkfield STEM image in Fig. 14, is calcite, ~0.5 to 1 µm in thickness, which crosscuts the host melilite, as shown in the inset. Calcite is the only phase identified within the vein in this area, and it does not appear to have affected the melilite composition, which is the same (~Åk23) on both sides of the calcite vein. We infer that other veins in Fig. 13 are also composed of calcite. Calcite has been reported previously in Leoville (Abreu and Brearley 2005; Ash et al. 2002; Caillet and Buseck 1992; Komorowski Caillet et al. 2007; Sylvester et al. 1993), generally as a minor isolated phase or in veins.

As shown in Fig. 13, the calcite vein crosscuts the boundary clinopyroxene but terminates at the spinel. Figure 15, a view of the spinel-melilite interface at the opposite end of the Leo1 FIB section from the calcite vein, shows that calcite also occupies the interface region with spinel where it forms contacts with spinel, glass, clinopyroxene, and perovskite. In other areas near the interface, not shown in Figure 15, calcite lies between spinel and melilite. Since the calcite veining is prominent in the melilite (Figs. 13–14), we interpret this to mean that calcite precipitated opportunistically along existing fractures and that fracturing in the interface region was predominately, but not exclusively, along the spinel-clinopyroxene contact. In Leo1, both calcite and clinopyroxene are in contact with spinel, while glass is adjacent to the melilite. Note that glass-melilite contacts are irregular (i.e., rough interface boundaries), but calcite-spinel contacts are smooth. The presence of perovskite is consistent with the occasional hot spot in Ti maps of spinel reported by Paque et al. (2007a) and the observation of Caillet et al. (1993) that spinels in Leoville 3537-2 are commonly decorated by perovskites. The glass composition (17 wt% MgO, 36% Al_2O_3, 41% SiO_2, and 7% CaO) for the interface region of spinel grain Leo1 is similar to that of the glass in Leo2.

DISCUSSION

We order this discussion largely in reverse of the chronological order that created the interfacial regions between spinel and melilite, saving for last an analysis of boundary clinopyroxenes, which occur in both Allende TS-34 and Leoville 3537-2. We begin by first considering the significance of calcite veining in melilite near the spinel grain Leo1, which we infer to have been a late fracture filling event that generally had little effect on the compositions of other phases present. We then evaluate the possible influence of melilite alteration events and the significance of glass veins and the associated hydrated crystalline phase around Leoville spinels. Our principal objective here is to answer two simple questions: How did the glasses form, and what was the nature

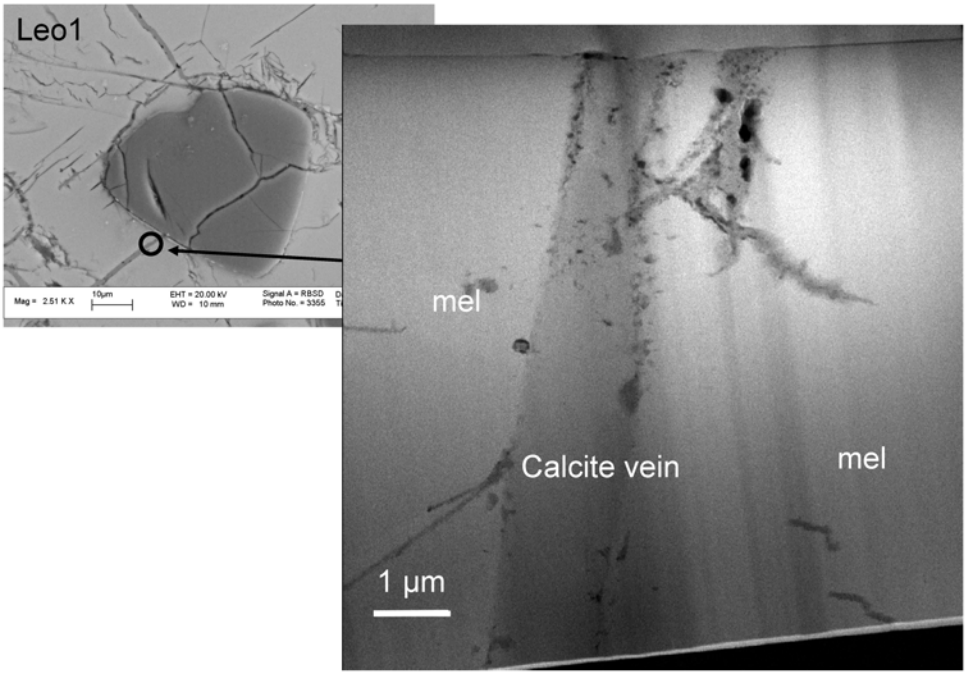

Fig. 14. Darkfield STEM image across calcite vein in melilite near Leoville 3537-2 spinel Leo1. The location of the TEM image (right) is indicated by the circle on the backscattered electron image (left). Scale bar is 10 μm in the upper left image and 1 μm in the lower right.

of the precursor? Finally, we address the origin of boundary clinopyroxenes, their relationship to coarser-grained pyroxenes, and their significance for thermal processing of type B1 inclusions.

Calcite

In meteorites, calcite is a secondary phase that could have formed in both terrestrial and extraterrestrial environments. In Leoville, which is a lightly weathered find, some of the calcite is unambiguously terrestrial, because it forms veins crosscutting the fusion crust, which formed during passage through the Earth's atmosphere, long after any parent body alteration (Abreu and Brearley 2005). On the other hand, Caillet and Buseck (1992) argued that calcite partially replaced wollastonite in a Leoville CAI in a process that appears to have predated the mechanical deformation events and was in fact preterrestrial. The thin, ~1 μm wide veins of calcite we observe around spinel grain Leo1, and occasionally other localities in the inclusion, fill polygonally fractured melilite but are not observed to reach the Wark-Lovering rim or to cross the inclusion boundary into the matrix. The veins are not associated with additional secondary phases that might hint at the point of origin and, in contrast to the glass veins discussed below, they do not appear to corrode melilite at calcite-melilite contacts. Thus, while it is possible that the calcite we observe in Leoville 3537-2 is preterrestrial, we exclude it from consideration of conditions in the Leoville parent body or in the primitive solar nebula. Its importance lies in possible effects of the altering medium, whether asteroidal, nebular, or terrestrial, on the compositions of previously existing phases.

The lack of additional phases in the veins (Figs. 13–14) is consistent with precipitation in fractures from relatively low-temperature aqueous fluids without significant dissolution or precipitation of other crystalline phases. It is also possible that water, which appears to be present in the interfacial glass and the unidentified Mg-, Al-, OH-rich crystals in Leoville 3537-2, as discussed above, was a product of the same event. Calcium could have been leached from the glass to form calcite but, based on exposed areas visible in the section, the amount of calcite in the general vicinity of Leo1 greatly exceeds the area of glass, and we therefore infer that Ca in the calcite is more likely to have been brought in with the fluid from an external source. Moreover, we see no evidence for dissolution of melilite in contact with calcite or of the precipitation of additional phases on the melilite (Fig. 14). Melilite in contact with glass in the interface region appears corroded (Fig. 15; see also Fig. 11a); areas in contact with calcite are generally smooth. In addition, we show below that compositions of glass associated with Leo1 and Leo2 are consistent with no significant loss or gain of Ca postdating glass formation. Thus, we infer that the alteration event involving the calcite around Leo2 postdated formation of the other phases and that it had no significant effect on the compositions of the previously existing phases with the caveat that hydration of the glass may have occurred during the same event.

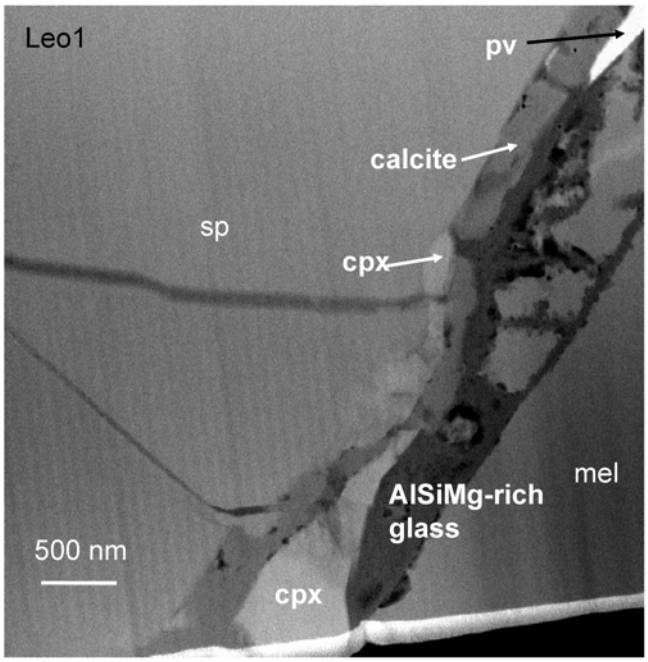

Fig. 15. Darkfield STEM image of spinel-melilite interface region of Leoville 3537-2 spinel Leo1. Scale bar is 500 nm. Perovskite (pv). Other abbreviations as in the caption to Fig. 6.

Formation of Leoville Glass Veins

Both Leo1 and Leo2 have glass veins between melilite and pyroxene or spinel. Other CAIs or Ca-Al-rich fragments in matrix in carbonaceous chondrites are known to have glass (El Goresy et al. 2002; Gray et al. 1973; Ireland et al. 1991; Kurat 1975; Marvin et al. 1970; Reid et al. 1974), but their compositions are strikingly different. In Figure 16a, a "Stolper" projection (Stolper 1982), CAI glass compositions are projected from spinel ($MgAl_2O_4$) onto the plane formed by the compositions of gehlenite ($Ca_2Al_2SiO_7$), anorthite ($CaAl_2Si_2O_8$), and forsterite (Mg_2SiO_4). CAI glass compositions taken from the literature form an arc in this projection anchored by the anorthite and gehlenite vertices (for a discussion on the application of projections to CAIs, see Beckett et al. 2006). Most are glass-rich objects, perhaps originally crystals or inclusions melted in high-velocity impacts in the primitive nebula, as discussed by Stolper (1982), but there are also examples of glass as a minor constituent in types A and B inclusions (El Goresy et al. 2002; Gray et al. 1973). The composition of glass from experiment 98-53, which is also shown in Fig. 16a, plots along this arc near the clinopyroxene-spinel-anorthite-melilite invariant point. Note that the 98-53 glass was a trapped liquid produced through fractional crystallization of melilite, and its composition plots close to the equilibrium saturation surface for melilite + spinel (see also Stolper and Paque 1986). We infer that residual liquids trapped by crystallizing melilite should plot near a melilite-saturated phase field or a short extension of it. Failure of a stable phase to nucleate can lead to continued metastable crystallization of a phase that is already crystallizing. However, even allowing for the uncertainties in the TEM EDS analyses, compositions of glass in the veins around Leo1 and Leo2 project far away from the arc for literature CAI glasses in Fig. 16a or its extensions and well away from the spinel + melilite multiply saturated liquidus phase field. The possible incorporation of melilite or clinopyroxene into the analyzed volume would move the projected compositions towards the spinel + melilite liquidus phase field, not away from it. Incorporation of spinel in the analysis volume would raise the "elevation" of the composition but have little effect on the projected position. Thus, it is likely that either a different process produced the Leoville glasses or that precursors to the Leoville glasses were very different from those of glasses from CAIs previously described in the literature.

As noted in the previous paragraph, the Leoville glass compositions are well removed from the melilite-saturated liquidus surface, which would be odd for a liquid nominally produced as a residual liquid during crystallization of melilite. In this brief section, we therefore undertake a formal assessment of fractional crystallization sequences of the Leoville glasses. If this material is derived from melt inclusions in melilite, then melilite should appear somewhere in the crystallization sequence. Figure 16b, which is a spinel projection onto the plane formed by the compositions of forsterite (Mg_2SiO_4), anorthite ($CaAl_2Si_2O_8$), and silica (SiO_2), is designed for more silica-rich compositions than Stolper's (1982) diagram and is therefore more suitable for a discussion of phase equilibria relevant to the Leoville glasses. Both phase diagrams share the plane anorthite-forsterite-spinel, which in projection plots as a line. Both are projected from $MgAl_2O_4$ spinel, which means that variable amounts of spinel component in the bulk composition have no effect on the projected composition. Figure 16b also shows the spinel-saturated liquidus surface after Sheng et al. (1991) and Sheng (1992) (also shown in Beckett et al. [2006]), contoured in wt% spinel component. Spinel is the liquidus phase for bulk compositions with wt% spinel component greater than that on the surface in the same projected position, and some other phase is on the liquidus for lower amounts of spinel. The compositions of Leo1 and Leo2 glasses are 15–20 wt% spinel component above the saturation surface and, therefore, spinel is the liquidus phase. Figure 16b can be used to infer crystallization sequences for spinel-saturated liquids that plot on the diagram and compositions of their residual liquids (see Beckett et al. [2006] for a discussion). For the Leo1 glass, the fractional crystallization sequence would be spinel → anorthite → cordierite → olivine and, for the Leo2 glass, spinel → cordierite → anorthite → olivine; crystallization paths for residual liquids derived from crystallization of both glasses are shown in gray.

A fundamental observation comes from an examination

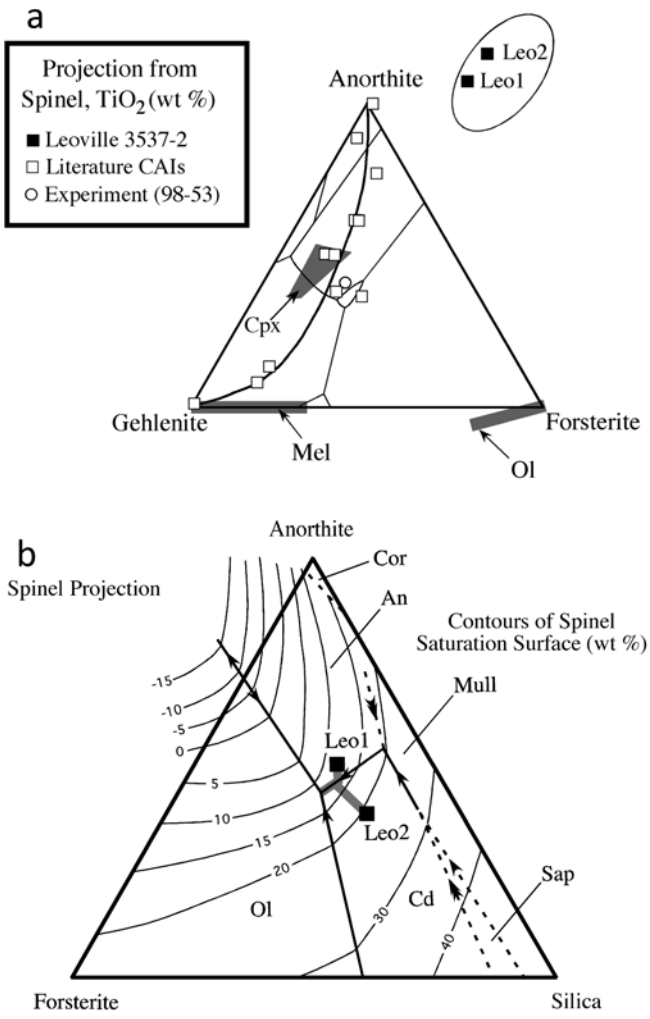

Fig. 16. Composition relationships of glass veins in Leoville. a) Projection of glass compositions from $MgAl_2O_4$ spinel onto the plane formed by the compositions of gehlenite ($Ca_2Al_2SiO_7$), anorthite ($CaAl_2Si_2O_8$) and forsterite (Mg_2SiO_4). Also shown are Al-rich glass compositions from the literature (El Goresy et al. 2002; Gray et al. 1973; Ireland et al. 1991; Kurat 1975; Marvin et al. 1970; Reid et al. 1974), projected composition volumes for clinopyroxene (Cpx), melilite (Mel), and olivine (Ol), and spinel-saturated multiply saturated boundary curves after Stolper (1982). An arc is drawn through the projected glass compositions as a visual aid. Note that the black Leo 1 and Leo 2 squares enclosed in an ellipse in the upper right portion of the diagram are data points, not part of a legend. b) Projection of Leoville glass compositions from $MgAl_2O_4$ spinel onto the plane formed by forsterite (Mg_2SiO_4), anorthite ($CaAl_2Si_2O_8$), and silica (SiO_2). Also shown is the spinel-saturated liquidus surface after Sheng (1992), contoured in wt% spinel component, with spinel-saturated liquidus phase fields for olivine (Ol), anorthite (An), corundum (Cor), mullite (Mull), cordierite (Cd), and sapphirine (Sap). Projected compositions of residual liquids produced on fractional crystallization of Leo1 and Leo2 glasses are shown in gray.

of the crystallization sequences for the Leoville glasses. Even when allowance is made for uncertainties in the TEM EDS analyses and possible contamination by other phases in the analyzed volume, all of which would either have no effect (spinel) or pull the composition towards the melilite field (melilite, clinopyroxene), melilite is completely absent from the crystallization sequence. It would be highly unusual for a trapped liquid around a spinel inclusion incorporated into a crystallizing melilite to be undersaturated with respect to the host phase. At the time a melt inclusion is trapped in a crystal, the liquid is generally saturated or even supersaturated with respect to the host phase, and it invariably crystallizes on the walls of the melt inclusion (cf. Gaetani and Watson 2000; Streck and Wacaster 2006) as is observed for the run product 98-53 described above. Thus, if the Leoville glasses are residual liquids from melt inclusions captured by melilite, we would expect melilite to appear in the crystallization sequence. Yet this is not the case for either of the Leoville glasses. Both glass compositions plot on the silica-rich side of the anorthite-forsterite-spinel join, which is a thermal divide for spinel-saturated liquids. Compositions close to, but on the silica-poor side of this join, will evolve toward melilite-saturated melts (e.g., olivine or anorthite crystallization from liquids near to, but on the silica-poor side of the join, will move them away from the join) and ultimately, the residual liquids will approach the spinel-saturated clinopyroxene and melilite stability fields (Fig. 16a). Similarly, olivine or anorthite crystallization from liquids near to, but on the silica-rich side of the join, will move residual liquid compositions further away from the join and, in particular, further away from the melilite-saturated phase field. Both of the Leoville glasses are well to the silica-rich side of the thermal divide (Fig. 16b). Neither will produce a residual liquid composition on the other side of the join through fractional or equilibrium crystallization and, therefore, neither of them is a residual liquid from the melilite-rich side of the thermal divide. Indeed, the glass compositions can be described in terms of positive amounts of anorthite, forsterite, spinel and cordierite, which is consistent with the anorthite-forsterite-cordierite-spinel-liquid invariant point being a eutectic composition. The compositions of Leo1 and Leo2 glasses are in the general vicinity of this invariant point in Fig. 16b, but the spinel contents are well above the saturation surface and there is no evidence for the presence of cordierite in Leoville 3537-2 or of igneous olivine for that matter (i.e., these are not near-eutectic liquids).

The absence of anomalies in melilite composition near the glass veins is also inconsistent with a partially crystallized residual liquid. Had the glass been a quenched residual liquid, strong zoning would have been expected near the interface with the glass as is seen in experimentally produced synthetic glass. Such zoning is not observed in the Leoville glasses.

The Leoville glasses are not residual liquids produced through fractional crystallization and, in particular, they are not residual liquids produced during the crystallization of melilite.

In the preceding paragraphs, we used a phase diagram to infer crystallization sequences for the Leoville glasses. The

saturation surface can also be contoured in temperature and this leads to the conclusion that high temperatures (>~1325 °C) would be needed to melt anhydrous precursor materials of the Leoville glasses. We can also use Berman's (1983) thermodynamic model to estimate the liquidus temperatures as 1541 °C (Leo2) and 1611 °C (Leo1), spinel being the liquidus phase in both cases. All of these temperatures are quite high, and if the entire inclusion had been subjected to them, most or all of it would have melted. This implies an event that was extremely local in its thermal effects and did not involve the bulk of the inclusion.

Based on the above discussion, we infer that glasses from Leoville 3537-2 are not quenched remnants of residual liquids produced during crystallization of the host melilite, so we remain with the two simple questions posed at the beginning of the Discussion: How did the glasses form, and what was the nature of the precursors? A possible answer to the first question is that the Leoville glasses are the product of a locally enhanced pressure regime formed during a shock event whose peak pressure in the major phases was too low to cause significant heating effects. Leoville has a well-defined foliation with elongation of chondrules and inclusions (e.g., Cain et al. 1986). Inferred peak pressures for the bulk meteorite are <20 GPa (Nakamura et al. 1992), which would not be expected to lead to widespread melting. Shock waves are, however, notorious for producing local melting along grain boundaries and highly variable effects in heterogeneous, especially porous, materials by frictional heating (e.g., Kieffer et al. 1976; Sharp and DeCarli 2006; Stöffler et al. 1988). Where a shock wave passes through a porous material, or through a grain boundary between two dissimilar materials, considerable increases in peak pressures may be attained relative to ambient values nearby due to compaction effects and differences in the mechanical impedance of materials at grain boundaries (e.g., Sharp and DeCarli 2006).

We envision the precursor to a glass vein as a thin, porous layer of altered, possibly hydrated material, that was shocked to a peak pressure enhanced relative to pressures achieved in the other phases in the inclusion. On pressure release, the waste heat produced by shock in the vein region led to a large temperature increase with melting of the phases present. After shock heating, the ~1 μm thick veins cooled nearly instantaneously, leaving the observed glass. If the alteration assemblage was anhydrous, rather high local temperatures, ≥1550–1650 °C would have been required and probably quite large enhancements in peak pressure. If the phase assemblage was hydrous, required melting temperatures would have been lower, and possibly much lower, and required enhancements in peak pressures relative to those achieved in melilite correspondingly less.

We can place some constraints on the nature of the precursor material through an analysis of the glass compositions shown in Fig. 16b. One endmember is likely to be a composition that projects to or near the silica vertex in Fig. 16b. Candidates include the Mg-Al-silicates sudoite ($Mg_2Al_4Si_3O_{10}(OH)_8$); Mg-carpholite ($MgAl_2Si_2O_6(OH)_4$); chloritoid ($MgAl_2SiO_5(OH)_2$); and cordierite ($Mg_2Al_4Si_5O_{18}$), which plot at the silica vertex (i.e., Ca-free phases with molar ratio of Mg:Al = 2:1), and zeolites (Wlotzka and Wark 1982); sapphirine $(Mg,Al)_8(Al,Si)_6O_{20}$); and clinochlore ($Mg_5Al_2Si_3O_{10}(OH)_8$), which plot along the forsterite-silica join in Fig. 16b, ~15–30% of the way towards the forsterite vertex. The weight ratio of the silica to spinel components in the glasses allows a more specific assessment for potential endmembers plotting at the silica vertex. The Leo1 and Leo2 glasses yield 0.62 and 0.81 for this ratio, respectively, close to the values for the chlorite endmember sudoite (0.63) and the chain silicate Mg-carpholite (0.84). Cordierite (1.22) would be less consistent with the glass compositions; chloritoid (0.422) is possible but would require additional and substantial spinel content. The silica-poor endmember appears to be consistent with aluminous diopside. Clinochlore and sapphirine are inconsistent with pyroxene or melilite dominating at the silica-poor end of a mixture although other phases might be possible. Wlotzka and Wark's (1982) zeolite is a possible endmember but it would require large amounts of spinel (~40 wt%), which is quite refractory, and negative amounts of Ca-Tschermak's molecule ($CaAl_2SiO_6$) in the pyroxene. Compositions of the Leo1 and Leo2 glasses can, however, be described in terms of positive amounts of Mg-carpholite, spinel, Ca-Tschermak's molecule and diopside. Replacing Mg-carpholite by sudoite requires negative amounts (but probably within error of zero) of Ca-Tschermak's molecule for Leo1 glass. Thus, mass balance suggests that Mg-carpholite or sudoite and an aluminous diopside are consistent, to first order, with the glass compositions. These phases could be produced through the alteration of melilite in the interface region between spinel and melilite with cracks providing access, and this would be consistent with the observed corroded contacts between Leoville glasses and melilite. Both Mg-carpholite and sudoite are low-temperature phases, restricting the alteration process to temperatures <~400 °C (Fransolet and Schreyer 1984; Vidal et al. 2001; Wei and Powell 2006). Assuming Al to be immobile, this process would have required the loss of ~1/3 of the original Ca from the melilite (~Åk25) being altered with ~1/3 of Mg and Si in the alteration products being introduced from outside the interface region. If either Mg-carpholite or sudoite was, in fact, the Si-rich endmember, then the assemblage was hydrated, which as noted above could have important consequences in a shock event and also imply a significant partial pressure of H_2O. The alteration process would probably require the gain of Mg, Si, and water, presumably through transport in a vapor or aqueous solution along cracks. If this scenario is correct, then preterrestrial alteration of Leoville CAIs did occur although, based on the spatially limited glass, the extent was very modest. It was a

shock subsequent to this alteration event that led to melting in the vein due to the anvil effect of the melilite-spinel contact region, the porous nature of the alteration material and the presence of water, which could have greatly reduced the required peak pressure for melting.

A fundamental implication of our analysis is that the Leoville glass is not recording an igneous event in which the major igneous phases in the inclusion were participating.

Although Allende CAIs are more altered overall, Leoville spinel-melilite contact regions are more complex than those of Allende because of processes that occurred after the formation of the boundary clinopyroxenes. This suggests that the process(es) producing boundary clinopyroxenes may have been the same in both Allende and Leoville type B1 inclusions and that, somewhat surprisingly, the origin of boundary clinopyroxene may be better constrained via study of Allende CAIs, where alteration and shock effects along the boundaries with spinel appear to be absent.

Unidentified Crystal

The glass vein around spinel grain Leo1 contains an Mg-, Al-, OH-rich crystalline phase (Fig. 15). If, as supposed above, this is a layered double hydroxide, it seems likely that the phase formed after the shock event that produced the glass. Otherwise, one would have to postulate that this extremely water-rich phase survived a shock event intact while the precursor phase(s) to the glass was completely vitrified. It is possible that the unidentified phase crystallized from the glass or condensed from a vapor during cooling following the shock. An alternative, perhaps the most likely one, is that this phase is a terrestrial alteration product of the glass. Although the origin of the unidentified crystal remains to be determined, it formed after the completion of all igneous processing.

Boundary Clinopyroxenes

In a previous subsection, we rejected the possibility that glass veins in Leoville are a product of residual liquids produced during crystallization of melilite, but the idea that boundary clinopyroxenes crystallized from residual liquids (i.e., from melt inclusions along spinel-melilite boundaries) also needs to be carefully considered. In this section, we first evaluate the possible crystallization of boundary clinopyroxenes from residual liquids and then briefly consider shock melting. We believe that these processes were not responsible for the formation of boundary clinopyroxenes in either Allende TS-34 or Leoville 3537-2. We then evaluate two alternatives that we believe to be more plausible and suggest that both may have been operative. The first is that some boundary clinopyroxenes are a consequence of either direct dissolution of perovskite (clinopyroxene later crystallized in regions of melt with enhanced concentration of Ti produced by the dissolution of perovskite) or indirect dissolution of perovskite (clinopyroxene formed a reaction rind between perovskite and liquid). The second is that some boundary clinopyroxenes are relict crystals relative to the most recent melting event.

There are several reasons why it is unlikely that boundary clinopyroxenes generally formed from residual liquids within melt inclusions, including the following:

(1) As discussed in the Results section, careful analytical searches in the vicinity of spinel grains with boundary clinopyroxene show small gradients in melilite composition both on melilite-spinel and on melilite-boundary clinopyroxene contacts. Similarly the FIB/SEM data in Figure 7c show a thin rind of zoned melilite between boundary clinopyroxene in the core of the inclusion and host melilite, although such rinds are absent for mantle spinel inclusion E2 (Figure 6b). For crystallization of melt inclusions around spinel grains in TS-34 mantle melilite of composition Åk22 to Åk35, frequent observations of high Åk values (Åk40 to Åk60) would be expected, but these were never observed. Independent of boundary clinopyroxene, the presence of spinel is associated with small perturbations in the composition of the surrounding melilite. These small changes contrast with compositions of melilite in the experimental run product, which are characterized by large increases in Åk content near glass-melilite or clinopyroxene-melilite contacts (Fig. 1b). Although conceivably important (as well as high-Åk “hot spots” observed within apparently pure melilite regions), we conclude that these small Åk variations of unknown origin in melilite adjacent to boundary clinopyroxene do not support the origin of the boundary clinopyroxene by crystallization of a melt inclusion. Whatever the origin of the boundary clinopyroxene, it is likely that there would be some small compositional perturbations in the surrounding melilite.

For spinel inclusions in core melilite, where large clinopyroxene crystals are co-crystallizing with melilite and anorthite, small spinel-melilite boundary clinopyroxene grains may be plausible as representatives of the last drops of the original liquid with pyroxene-like compositions, but here the adjacent melilite might be expected to have unusually high Åk values, which is not observed. Moreover, given the fact that pyroxene was crystallizing elsewhere, a simpler explanation is that the boundary pyroxene nucleated on the spinel and was then incorporated sans melt into crystallizing melilite. In any case, as emphasized below, the boundary clinopyroxenes on spinel inclusions in mantle melilite represent the largest interpretational challenge because they are enclosed in aluminous, presumably early crystallizing melilite with liquid compositions greatly undersaturated with respect to clinopyroxene.

(2) Even if the issue of melilite zoning is ignored, residual liquid compositions produced by fractional crystallization of melilite in type B CAIs are not exactly

equivalent to melilite + clinopyroxene ± spinel. This is shown in the residual glass compositions from the present experimental study. We would therefore expect to at least occasionally encounter additional phases that co-crystallized with the boundary clinopyroxenes and, aside from the occasional perovskite crystal, which does not solve the mass balance discrepancy, we never do. This is particularly true of boundary clinopyroxenes in the mantle, for which potential melt inclusions would be expected to have compositions well removed from those of the pyroxene. Yet, glass or additional crystalline igneous phases such as anorthite are not observed. The absence of anorthite is especially significant, as this phase is present in essentially all type B CAIs. It is widely accepted that anorthite nucleation is delayed relative to clinopyroxene in crystallization of type B CAI compositions, but late is not never, and some boundary anorthite should have been found along with clinopyroxene if these features formed by crystallization of melt inclusions in melilite.

(3) For spinel inclusions in mantle melilite, primary crystallization cannot explain the presence of the Ti-rich boundary clinopyroxenes unless present ideas on the equilibrium crystallization sequence of type B CAIs are incorrect, because clinopyroxene appears late in the fractional crystallization sequence, after the Ti content of the melt has been enhanced by considerable fractional crystallization of the low Ti phases, spinel and melilite (e.g., Stolper 1982). The same problem exists for coarse mantle clinopyroxenes that are not obviously associated with spinel. One could appeal to clinopyroxene crystallization following failure of melilite (as well as anorthite) to nucleate, but there is no evidence for this in a large number of dynamic crystallization experiments conducted for a broad range of bulk compositions and run conditions (Beckett et al. 1990; Beckett and Stolper 2000; MacPherson et al. 1984; Maharaj and Hewins 1995, 1997; Paque and Stolper 1984; Stolper and Paque 1986; J. M. Paque, unpublished data). Supercooling followed by rapid disequilibrium growth of mantle melilite might be possible, and indeed apatite crystals attributed to this effect are occasionally observed in terrestrial rocks (Bacon 1989), but it is not obvious that the boundary layer liquid would be depleted in melilite components to the extent that clinopyroxene crystallization would result. Moreover, at least in the mantle, this would require very large enhancements in the Ti (also Sc) concentration of the liquid at the interface, for which there is no experimental evidence.

In the preceding subsection, we argue against the formation of boundary clinopyroxenes through crystallization of trapped liquids. Shock melting also appears unlikely given the similarity in composition between the boundary clinopyroxenes and coarser-grained pyroxenes in the same region of the inclusion and the absence of sufficient Ti near spinel-melilite interfaces to produce the clinopyroxene. Shock melting of a spinel-melilite mixture could not provide the high Ti seen in the boundary clinopyroxenes. Even if one were to presuppose that shock melting somehow led to the formation of the boundary clinopyroxenes, this would fail to explain, especially in the mantle, the presence of essentially equivalent, and in many cases larger, clinopyroxenes that are not associated with any spinel, which would therefore have had a different and presumably lower peak pressure. It would also fail to account for the enrichment in Sc and rare earth element (REE) concentrations commonly observed in mantle clinopyroxenes (e.g., Simon et al. 1991).

An alternative scenario for the formation of boundary clinopyroxenes, particularly in the mantle, is that perovskite dissolution led to the crystallization of clinopyroxene. If perovskite underwent “direct dissolution,” it would have bled Ti into the melt, with the locally enhanced Ti concentrations leading to later crystallization of clinopyroxene during cooling before the melt homogenized with nearby Ti-poor liquid. An alternative is “indirect dissolution,” which occurs when a phase reacts with a liquid to form one or more intermediate phases between the dissolving phase and liquid. In this case, clinopyroxene would be viewed as a reaction product between perovskite and spinel plus liquid. Moreover, since the Ti necessary for growth of these Ti-rich pyroxenes would be limited to a small volume of melt in the immediate vicinity of the dissolving or dissolved perovskite seed, the size of any resulting clinopyroxene grain would be limited by the supply of dissolving perovskite. Taking the limiting case of all Ti in the perovskite being retained by the clinopyroxene, the volume of product clinopyroxene would be about 4 to 6 times that of the original perovskite. Thus, a 1 μm perovskite grain could produce an ~5 μm clinopyroxene, which is consistent with observed dimensions of perovskite crystals and boundary clinopyroxenes. Moreover, if such a grain of clinopyroxene, having grown in the locally Ti-enhanced liquid, were to continue to be exposed to the surrounding, progressively less saturated melt, it would ultimately dissolve away unless the temperature decreased sufficiently to stabilize clinopyroxene, or it was captured by a crystallizing melilite (more likely, at least in the mantle). It is worth noting that mantle clinopyroxenes do not show crystal terminations even though nearby crystals are unlikely to have impeded growth prior to incorporation into melilite. Both the isolated, sometimes large, spinel-free clinopyroxenes and the boundary clinopyroxenes in the mantle are generally rounded/resorbed, consistent with partial dissolution (Simon and Grossman 2006; Simon et al. 1991).

The above model is supported by the observation of epitaxial perovskites on the surface of some spinel crystals from Allende inclusions (Barber et al. 1984).

Kennedy et al. (1997) appealed to a perovskite dissolution mechanism to explain low REE concentrations in mantle melilites of Allende type B1 inclusion USNM 3655A. Their idea was that perovskite sequestered much of the REE budget for the inclusion during the initial stages of melilite crystallization and that as perovskite dissolved into the liquid,

REE concentrations in the liquid rose. Kennedy et al. (1997) observed perovskite in the mantle of 3655A, and they commonly decorate spinel crystals in the mantle of Leoville 3537-2 (Caillet et al. 1993; Connolly and Burnett 1999). Ti-rich clinopyroxenes rimming rounded perovskite grains are relatively common in compact type A (CTA; very melilite-rich) inclusions and, indeed, both El Goresy et al. (2002) and Lin et al. (2003) interpreted such grains as having grown on dissolving perovskite cores. It is worth noting that compositions of mantle clinopyroxenes in type B1 inclusions are very similar to those in type A inclusions, and it is not unreasonable to surmise that a similar process may have produced both. The difference for mantles of type B1 inclusions may be that the perovskite, which was present initially, dissolved completely or nearly completely prior to the nucleation of clinopyroxene due either to smaller average perovskite grain sizes than in type A inclusions, or to more intense heating. The arguments given above apply specifically to mantle clinopyroxenes and, given the relatively low Ti contents of boundary clinopyroxenes in the core, the similarity of their compositions to nearby coarse-grained clinopyroxenes, the differences in composition relative to clinopyroxenes from the mantle, and the rarity of perovskite decorating spinel in the core compared to the mantle, it seems unlikely that perovskite dissolution can account for both.

In detail, the chemistries of perovskite and mantle clinopyroxenes are probably inconsistent with a scenario that produces mantle clinopyroxenes solely through crystallization around a dissolving or completely dissolved perovskite. At least in compact type A inclusions (El Goresy et al. 2002; Fahey et al. 1987), perovskite, the presumed precursor, has generally lower Sc/Ti (0.001–0.015 versus 0.001–0.11) and Sc/Zr (0.03–0.5 versus 0.6–2.1) and higher Y/Sc (0.8–17 versus 0.004–0.21) and Y/Zr (0.2–1.3 versus 0.02–0.15) than does clinopyroxene in CTAs (Simon et al. 1999) or the mantle of TS-34 (Simon et al. 1991). We would not expect an exact match, as the clinopyroxene must partition elements from the liquid and, as the trace elements are released from the perovskite, they diffuse at different rates in the melt. However, neither variable diffusion rates (faster for trivalent cations than for tetravalent cations) nor differences in apparent partition coefficients for clinopyroxene-liquid (Simon et al. 1991) seem likely to account for the differences in concentration ratios of elements between perovskite and mantle pyroxene. This suggests, in the context of a perovskite dissolution model, that an additional, now generally absent Sc-Zr-rich, Y-poor phase or phases was involved. Weber and Bischoff (1994) described a mineral included in a perovskite-rich CAI (approximately $Sc_4Zr_3O_{12}$) that has the right characteristics (high Sc and Zr with low Y; also Ma (2008, personal communication) observed this phase as the principle constituent of an Allende inclusion). Such a phase would also be expected to have low REE contents, consistent with low enrichments of the REE in the mantle clinopyroxenes of TS-34 (Simon et al. 1991). Thus, dissolution of perovskite, either rimmed by or intimately associated with a Sc-Zr-rich oxide, could explain the observed chemistries of clinopyroxene surrounding perovskite in CTAs and of isolated clinopyroxenes in the mantles of type B1 inclusions. Both Ti^{3+} and Sc are highly compatible in clinopyroxene (e.g., Hill et al. 2000; Simon et al. 1991) and the enhanced concentrations of these elements in mantle clinopyroxenes would be expected to stabilize clinopyroxene relative to Ti^{3+}-Sc free pyroxenes in otherwise compositionally equivalent CAI-like liquids. This equilibrium stabilization is probably a modest effect, perhaps 10–20 °C based on data of Stolper et al. (1982) and Beckett (1986). The important point is, however, that the appearance temperature of clinopyroxene during indirect dissolution of perovskite was likely close to the equilibrium appearance temperature (for the composition join between the dissolving perovskite and surrounding CAI liquids) whereas the appearance temperature for clinopyroxene in the core was likely suppressed by many tens to a hundred degrees or more due to nucleation effects (Stolper and Paque, 1986). This could have led to clinopyroxenes in the mantle appearing at much higher temperatures than those in the core.

There is mounting evidence that type B inclusions experienced more than one melting event (Beckett and Stolper 2000; Connolly et al. 2003; Ito et al. 2004; Lin and Kimura 2000; MacPherson and Davis 1993; Simon et al. 2005), and it is important to consider how complex thermal histories have affected boundary clinopyroxenes. Simon and Grossman (2006) showed that compositions of clinopyroxenes in the cores and mantles of type B1 inclusions are distinctive, with clinopyroxenes in the mantle generally Mg-poor and often Ti-rich relative to those in the core. We noted above that compositions of boundary clinopyroxenes in Allende TS-34 and Leoville 3537-2 are consistent with those of coarse-grained clinopyroxenes from the same portion of the inclusion. This suggests first that boundary clinopyroxenes and spinel-free coarser clinopyroxenes from the mantle share a common origin. The same may be true for the core, but processes in the two venues differed. We suggested above that boundary clinopyroxenes in the mantle were derived from crystallization in the wake of dissolving perovskite + Sc-oxide grains. In the core, perovskite decorating spinels was generally destroyed before it could influence the kinetics of pyroxene nucleation, though spinel may still have provided a favorable nucleation site. Patchy zoned clinopyroxenes thought to represent multiple heating/cooling events are observed in some type B1 inclusions (Davis et al. 1998; Paque 1990; although we note that complex zoning in pyroxene can be produced during simple single stage cooling as shown in Fig. 1a). Core clinopyroxenes frequently have resorbed textures (MacPherson et al. 1989), which is consistent with other lines

of evidence for multiple melting events. These observations hint at complex thermal histories in which pyroxenes in the core were periodically exposed to temperatures high enough to cause partial resorption. Based on phase equilibria (Stolper 1982), temperatures of 1250–1300 °C would have been sufficient to provoke wide-scale partial melting in the core without strongly affecting the mantle. Any clinopyroxene not armored by aluminous melilite would have potentially been exposed to the melt and partially to completely dissolved. Mantle clinopyroxenes, which are enclosed in aluminous melilite grains with higher melting points than the peak temperature of the later melting event, would not have been exposed to these new liquids and would therefore have retained the signature of the initital melting event.

There are both differences and similarities between boundary clinopyroxene and the large spinel-free clinopyroxenes in the mantle. Simon et al. (1991) report unusually high Åk melilite adjacent to large mantle clinopyroxene grains in TS-34, and we observed a gradient of decreasing melilite Åk with distance away from one of the two large mantle clinopyroxene grains in our TS-34 section. In contrast, we found no high Åk melilite adjacent to boundary clinopyroxenes despite an extensive search, and in the case of the FIB/STEM section for spinel grain Leo2, the lack of an anomalous composition gradient is observed on a 1–3 μm scale. Simon et al. (1991) interpreted a large mantle clinopyroxene in TS-34 as a relict grain surrounded by a melt inclusion (to explain the high Åk melilite adjacent to the mantle clinopyroxene). Our interpretation is only slightly different. We regard the large mantle clinopyroxene as forming from collections of relict perovskite and a Sc-Zr-rich, Y-poor phase ± spinel, not clinopyroxene. Moreover, we think that the Åk gradients with distance away from these large mantle clinopyroxenes are naturally produced as melilite crystallizes around a large clinopyroxene that is dissolving in the liquid. The same process was operative near the spinel-melilite boundary clinopyroxenes, possibly accounting for the small Åk gradients observed in our SEM/EPMA analyses or in FIB section B2-2 (Fig. 7c).

An important consequence of our interpretations is that all mantle spinels with boundary clinopyroxene, i.e., the majority of mantle spinels, are relict grains, perhaps nebular condensates decorated by perovskite Sc-oxide.

CONCLUSIONS

We characterized the interfacial region between spinel and host melilite in type B1 inclusions from the Allende and Leoville carbonaceous chondrites using FIB/STEM techniques. Boundary clinopyroxenes, both blebs and rinds, are common in both inclusions studied, but the Leoville occurrences are more complex with glass veins, possibly hydrated, between the melilite and pyroxene or spinel. Calcite, perovskite, and an unknown phase can also be present.

The Leoville glasses have compositions consistent with a precursor phase assemblage containing an aluminous diopside and Mg-carpholite or sudoite, and inconsistent with residual melt compositions derived from fractional crystallization of melilite. We infer that the glass formed by shock melting of an alteration phase assemblage concentrated in the interface region between spinel and melilite. It is quite striking that in this study the evidence for alteration effects near spinel-melilite interfaces comes from the Leoville sample and not from the Allende FIB/STEM sections. It has been previously concluded that all CV chondrites, both in reduced and oxidized subgroups, experienced alteration (see Krot et al. 1998 and references therein); it is the style and extent of alteration that differs among the various CAIs.

Boundary clinopyroxenes did not crystallize from residual melt pools trapped in melilite, as they lack strongly zoned melilite compositions near the interface, and additional phases that might be expected for late-stage crystallization are not observed. Moreover, the compositions of boundary clinopyroxenes are similar to those of coarse-grained clinopyroxenes from the same region of the inclusion. The divergence of phase compositions in mantle versus core extends from spinel and melilite compositions to clinopyroxenes. In the mantle, clinopyroxene may have either crystallized in local Ti-enriched melts generated by direct perovskite dissolution with a preference for nucleation on spinels, because perovskite often decorates the surface of these grains, or formed as a reaction product between perovskite and melt (indirect dissolution of perovskite).

Acknowledgments–Reviews by S. Simon and A. N. Krot were useful and appreciated. We thank Steve Simon and Larry Grossman for the loan of the section of TS-34 and Glenn MacPherson (Smithsonian Institution) for USNM Leoville 3537-2. This work was funded in part by NASA grants NNG04GG14G, NNG05GH797, and NAG5-11640. Portions of this work were also performed under the auspices of the U.S. Department of Energy by Lawrence Livermore National Laboratory in part under Contract W-7405-Eng-48 and in part under Contract DE-AC52-07NA27344.

Editorial Handling—Dr. Christine Floss

REFERENCES

Abreu N. M. and Brearley A. J. 2005. Carbonates in Vigarano: terrestrial, preterrestrial, or both. *Meteoritics & Planetary Science* 40:609–625.

Armstrong J. T. 1988. Quantitative analysis of silicate and oxide materials: Comparison of Monte Carlo, ZAF, and (z) procedures. In *Quantitative electron probe analysis*, edited by Newbury D. E. San Francisco: San Francisco Press. pp. 239–246.

Armstrong J. T., El Goresy A. and Wasserburg G. J. 1985. Willy: A prize noble Ur-Fremdling—Its history and implications for the formation of Fremdlinge and CAI. *Geochimica et Cosmochimica Acta* 49:1001–1022.

Ash R. D., Russell S. S., Belshaw N. C., Young E. D., and Gounelle M. 2002. Mg isotopes in melilite, fassaite, and spinels in CAIs: Evidence for evaporation, equilibration and late stage alteration (abstract #2063). 33rd Lunar and Planetary Science Conference. CD-ROM.

Bacon C. R. 1989. Crystallization of accessory phases in magmas by local saturation adjacent to phenocrysts. *Geochimica et Cosmochimica Acta* 53:1055–1066.

Barber D. J., Beckett J. R., Paque J. M., and Stolper E. 1994. A new titanium-bearing calcium aluminosilicate phase: II. Crystallography and crystal chemistry of grains formed in slowly cooled melts with bulk compositions of calcium-aluminum-rich inclusions. *Meteoritics* 29:682–690.

Barber D. J., Martin P. M., and Hutcheon I. D. 1984. The microstructure of minerals in coarse-grained Ca-Al-rich inclusions from the Allende meteorite. *Geochimica et Cosmochimica Acta* 48:769–783.

Beckett J. R. 1986. The origin of calcium-, aluminum-rich inclusions from carbonaceous chondrites: An experimental study. Ph.D. thesis. University of Chicago, Chicago, Illinois, USA.

Beckett J. R., Connolly H. C. Jr., and Ebel D. S. 2006. Chemical processes in igneous calcium-aluminum-rich inclusions: A mostly CMAS view of melting and crystallization. In *Meteorites and the early solar system II*, edited by Lauretta D. S. and McSween H. Y. Tucson: The University of Arizona Press. pp. 399–430.

Beckett J. R., Simon S. B., and Stolper E. 2000. The partitioning of Na between melilite and liquid: Part II. Applications to type B inclusions from carbonaceous chondrites. *Geochimica et Cosmochimica Acta* 64:2519–2534.

Beckett J. R., Spivack A. J., Hutcheon I. D., Wasserburg G. J., and Stolper E. M. 1990. Crystal chemical effects on the partitioning of trace elements between mineral and melt: An experimental study of melilite with applications to refractory inclusions from carbonaceous chondrites. *Geochimica et Cosmochimica Acta* 54: 1755–1774.

Beckett J. R. and Stolper E. 2000. The partitioning of Na between melilite and liquid: Part I. The role of crystal chemistry and liquid composition. *Geochimica et Cosmochimica Acta* 64:2509–2517.

Berman R. G. 1983. A thermodynamic model for multicomponent melts, with application to the system CaO-MgO-Al_2O_3-SiO_2. Ph.D. thesis. University of British Columbia, Canada.

Bernatowicz T. J., Amari S., Zinner E. K., and Lewis R. S. 1991. Interstellar grains within interstellar grains. *The Astrophysical Journal* 373:L73–L76.

Bleiner D., Macri M., Gasser P., Sautter V., and Maras A. 2006. FIB, TEM and LA-ICPMS investigations on melt inclusions in Martian meteorites—Analytical capabilities and geochemical insights. *Talanta* 68:1623–1631.

Blum J. D., Wasserburg G. J., Hutcheon I. D., Beckett J. R., and Stolper E. M. 1989a. Diffusion, phase equilibria and partitioning experiments in the Ni-Fe-Ru system. *Geochimica et Cosmochimica Acta* 53:483–489.

Blum J. D., Wasserburg G. J., Hutcheon I. D., Beckett J. R., and Stolper E. M. 1989b. Origin of opaque assemblages in C3V meteorites: Implications for nebular and planetary processes. *Geochimica et Cosmochimica Acta* 53:543–556.

Bradley J., Dai Z. R., Erni R., Browning N., Graham G., Weber P., Smith J., Hutcheon I., Ishii H., Bajt S., Floss C., Stadermann F., and Sandford S. 2005. An astronomical 2175 Å feature in interplanetary dust particles. *Science* 307:244–247.

Caillet C. and Buseck P. R. 1992. The "white angel": A wollastonite-bearing refractory inclusion in the Leoville chondrite (abstract). *Meteoritics* 27:208.

Caillet C., MacPherson G. J., and Zinner E. K. 1993. Petrologic and Al-Mg isotopic clues to the accretion of two refractory inclusions onto the Leoville parent body: One was hot, the other wasn't. *Geochimica et Cosmochimica Acta* 57:4725–4743.

Cain P. M., McSween H. Y., and Woodward N. B. 1986. Structural deformation of the Leoville chondrite. *Earth and Planetary Science Letters* 77:165–175.

Campbell A. J., Simon S. B., Humayun M., and Grossman L. 2003. Chemical evolution of metal in refractory inclusions in CV3 chondrites. *Geochimica et Cosmochimica Acta* 67:3119–3134.

Clayton R. N., Onuma N., Grossman L., and Mayeda T. K. 1977. Distribution of the presolar component in Allende and other carbonaceous chondrites. *Earth and Planetary Science Letters* 34:209–224.

Connolly H. C. and Burnett D. S. 1999. A study of the minor element concentrations of spinels from two type B calcium-aluminum-rich inclusions: An investigation into potential formation conditions of calcium-aluminum-rich inclusions. *Meteoritics & Planetary Science* 34:829–848.

Connolly H. C. Jr. and Burnett D. S. 2003. On type B CAI formation: Experimental constraints on fO_2 variations in spinel minor element partitioning and reequilibration effects. *Geochimica et Cosmochimica Acta* 67:4429–4434.

Connolly H. C. Jr., Burnett D. S., and McKeegan K. D. 2003. The petrogenesis of type B1 Ca-Al-rich inclusions: The spinel perspective. *Meteoritics & Planetary Science* 38:197–224.

Croat T. K., Stadermann F. J., and Bernatowicz T. J. 2005. Presolar graphite from AGB stars: microstructure and s-process enrichment. *The Astrophysical Journal* 631:976–987.

Daulton T. L., Bernatowicz T. J., Lewis R. S., Messenger S., Stadermann F. J., and Amari S. 2002. Polytype distribution in circumstellar silicon carbide. *Science* 296:1852–1855.

Daulton T. L., Bernatowicz T. J., Lewis R. S., Messenger S., Stadermann F. J., and Amari S. 2003. Polytype distribution of circumstellar silicon carbide: Microstructural characterization by transmission electron microscopy. *Geochimica et Cosmochimica Acta* 67:4743–4767.

Davis A. M., Simon S. B., and Grossman L. 1994. Alteration of Allende type B1 CAIs: When, where and how (abstract). 25th Lunar and Planetary Science Conference. pp. 315–316.

Davis A. M., Simon S. B., and Grossman L. 1998. Reexamination of the Allende type B1 CAI NMNH 5241 (abstract #1948). 24th Lunar and Planetary Science Conference. CD-ROM.

El Goresy A., Nagel K., and Ramdohr P. 1978. Fremdlinge and their noble relatives. Proceedings, 9th Lunar and Planetary Science Conference. pp. 1279–1303.

El Goresy A., Zinner E., Matsunami S., Palme H., Spettel B., Lin Y., and Nazarov M. 2002. Efremovka 101.1: A CAI with ultrarefractory REE patterns and enormous enrichments of Sc, Zr, and Y in fassaite and perovskite. *Geochimica et Cosmochimica Acta* 66:1459–1491.

Fahey A. J., Zinner E. K., Crozaz G., and Kornacki A. S. 1987. Microdistributions of Mg isotopes and REE abundances in a type A calcium-aluminum-rich inclusion from Efremovka. *Geochimica et Cosmochimica Acta* 51:3215–3229.

Floss C., Stadermann F. J., Bradley J., Dai Z. R., Bajt S., and Graham G. 2004. Carbon and nitrogen isotopic anomalies in an anhydrous interplanetary dust particle. *Science* 303:1355–1358.

Ford R. and Brearley A. J. 2007. Phyllosilicates in two coarse-grained Allende CAIs: Evidence for advanced hydration (abstract #2411). 38th Lunar and Planetary Science Conference. CD-ROM.

Fransolet A.-M. and Schreyer W. 1984. Sudoite, di/trioctahedral chlorite: a stable low-temperature phase in the system MgO-Al_2O_3-SiO_2-H_2O. *Contributions to Mineralogy and Petrology* 86:409–417.

Gaetani G. A. and Watson E. B. 2000. Open system behavior of olivine-hosted melt inclusions. *Earth and Planetary Science Letters* 183:27–41.

Giannuzzi L. A., Drown J. L., Brown S. R., Irwin R. B., and Stevie F. A. 1998. Applications of the FIB lift-out technique for TEM specimens preparation. *Microscopy Research and Technique* 41: 285–290.

Giannuzzi L. A. and Stevie F. A. 1999. A review of focused ion beam milling techniques for TEM specimens preparation. *Micron* 30: 197–204.

Gray C. M., Papanastassiou D. A., and Wasserburg G. J. 1973. The identification of early condensates from the solar nebula. *Icarus* 20:213–239.

Greshake A., Bischoff A., and Putnis A. 1998. Transmission electron microscope study of compact type A calcium-aluminum-rich inclusions from CV3 chondrites: Clues to their origin. *Meteoritics & Planetary Science* 33:75–87.

Grossman L., Ebel D. S., Simon S. B., Davis A. M., Richter F. M., and Parsad N. M. 2000. Major element chemical and isotopic compositions of refractory inclusions in C3 chondrites: the separate roles of condensation and evaporation. *Geochimica et Cosmochimica Acta* 64:2879–2894.

Grossman L., Ebel D. S., and Simon S. B. 2002. Formation of refractory inclusions by evaporation of condensate precursors. *Geochimica et Cosmochimica Acta* 66:145–161.

Grossman L, Simon S. B., Rai V. K., Thiemens M. H., Hutcheon I. D., Williams R. W., Galy A., Ding T., Fedkin A.V., Clayton R. N., and Mayeda T. K. 2008. Primordial compositions of refractory inclusions. *Geochimica et Cosmochimica Acta* 72:3001–3021.

Heaney P. J., Vicenzi E. P., Giannuzzi L. A. and Livi K. J. T. 2001. Focused ion beam milling: A method of site-specific sample extraction for microanalysis of Earth and planetary materials. *American Mineralogist* 86:1094–1099.

Hill E., Wood B. J. and Blundy J. D. 2000. The effect of Ca-Tschermak's component on trace element partitioning between clinopyroxene and silicate melt. *Lithos* 53:203–215.

Ireland T. R., Fahey A. J., and Zinner E. K. 1991. Hibonite-bearing microspherules: A new type of refractory inclusions with large isotopic anomalies. *Geochimica et Cosmochimica Acta* 55:367–379.

Ito M., Nagasawa H., and Yurimoto H. 2004. Oxygen isotopic SIMS analysis in Allende CAI: Details of the very early thermal history of the solar system. *Geochimica et Cosmochimica Acta* 68:2905–2923.

Keller L. P. and Buseck P. R. 1991. Calcic micas in the Allende meteorite: Evidence for hydration reactions in the early solar nebula. *Science* 252:946–949.

Keller L. P. and Buseck P. R. 1994. Twinning in meteoritic and synthetic perovskite. *American Mineralogist* 79:73–79.

Kennedy A. K., Beckett J. R., Edwards D. A., and Hutcheon I. D. 1997. Trace element disequilibria and magnesium isotope heterogeneity in 3655A: Evidence for a complex multi-stage evolution of a typical Allende type B1 CAI. *Geochimica et Cosmochimica Acta* 61:1541–1561.

Kieffer S. W., Phakey P. P., and Christie J. M. 1976. Shock processes in porous quartzite: transmission electron microscope observations and theory. *Contributions to Mineralogy and Petrology* 59:41–93.

Komorowski Caillet C. L. V., Zinner E. K., McKeegan K. D., Hervig R., and Buseck P. R. 2007. The white angel: A unique wollastonite-bearing, mass-fractionated refractory inclusion from the Leoville CV3 carbonaceous chondrite. *Meteoritics & Planetary Science* 42:1159–1182.

Kuehner S. M., Davis A. M., and Grossman L. 1989. Identification of relict phases in a once-molten Allende inclusion. *Geophysical Research Letters* 16:775–778.

Kurat G. 1975. Der kohlige Chondrit Lancé: Eine petrologische Analyses der komplexen Genese eines Chondriten. *Tschermaks Mineralogie Petrographie Mitteilung* 22:38–78.

Lee M. R., Bland P. A., and Graham G. 2003. Preparation of TEM samples by focused ion beam (FIB) techniques: applications to the study of clays and phyllosilicates in meteorites. *Mineralogical Magazine* 67:581–592.

Lin Y. and Kimura M. 2000. Two unusual type B refractory inclusions in the Ningqiang carbonaceous chondrite: Evidence for relicts, xenoliths and multi-heating. *Geochimica et Cosmochimica Acta* 64:4031–4047.

Lin Y., Kimura M. and Wang D. 2003. Fassaites in compact type A Ca-Al-rich inclusions in the Ningqiang carbonaceous chondrite: Evidence for partial melting in the nebula. *Meteoritics & Planetary Science* 38:407–417.

Lundstrom C. C., Sutton A. L., Chaussidon M., McDonough W. F., and Ash R. 2006. Trace element partitioning between type B CAI melts and melilite and spinel: Implications for trace element distribution during CAI formation. *Geochimica et Cosmochimica Acta* 70:3421–3435.

MacPherson G. J., Crozaz G., and Lundberg L. L. 1989. The evolution of a complex type B Allende inclusion: An ion microprobe trace element study. *Geochimica et Cosmochimica Acta* 53:2413–2427.

MacPherson G. J. and Davis A. M. 1993. A petrologic and ion microprobe study of a Vigarano type B refractory inclusion: Evolution by multiple stages of alteration and melting. *Geochimica et Cosmochimica Acta* 57:231–243.

MacPherson G. J., Paque J. M., Stolper E., and Grossman L. 1984. The origin and significance of reverse zoning in melilite from Allende type B inclusions. *Journal of Geology* 92:289–305.

Maharaj S. V. and Hewins R. H. 1995. Flash heating a type B CAI composition (abstract). 26th Lunar and Planetary Science Conference. pp. 883–884.

Maharaj S. V. and Hewins R. H. 1997. Effect of melt time and precursor phases on type B CAI textures (abstract #1624). 28th Lunar and Planetary Science Conference. CD-ROM.

Marvin U. B., Wood J. A., and Dickey J. S. 1970. Ca-Al rich phases in the Allende meteorite. *Earth and Planetary Science Letters* 7: 346–350.

Mendybaev R. A., Richter F. M., and Davis A. M. 2006. Crystallization of melilite from CMAS-liquids and the formation of the melilite mantle of type B1 CAIs: Experimental simulations. *Geochimica et Cosmochimica Acta* 70:2622–2642.

Müller W. F. 1978. Transmission electron microscope study of some minerals of the meteorite Allende (abstract). 9th Lunar and Planetary Science Conference. pp. 775–777.

Müller W. F. and Wlotzka F. 1982. Mineralogical study of the Leoville meteorite (CV3): Macroscopic texture and transmission electron microscopic observations (abstract). 13th Lunar and Planetary Science Conference. pp. 558–560.

Nakamura T., Tomeoka K., and Takeda H. 1992. Shock effects of the Leoville CV carbonaceous chondrite: a transmission electron microscope study. *Earth and Planetary Science Letters* 114:159–170.

Nguyen A. N., Stadermann F. J., Zinner E., Stroud R. M., Alexander C. M. O'D., and Nittler L. R. 2007. Characterization of presolar silicate and oxide grains in primitive carbonaceous chondrites. *The Astrophysical Journal* 656:1223–1240.

Obst M., Gasser P., Mavrocordatos D., and Dittrich M. 2005. TEM-specimen preparation of cell/mineral interfaces using focused ion beam milling. *American Mineralogist* 90:1270–1277.

Overwijk M. H. F., van den Heuvel F. C., and Bulle-Lieuwma C. W. T. 1993. Novel schemes for the preparation of transmission electron microscopy specimens with a focused ion beam. *Journal of Vacuum Science and Technology B* 11:2021–2024.

Palme H., Hutcheon I. D., and Spettel B. 1994. Composition and origin of refractory-metal-rich assemblages in a Ca, Al-rich Allende inclusion. *Geochimica et Cosmochimica Acta* 58:495–513.

Paque J. M. 1990. Relict grains in a Ca-Al-rich inclusion from Allende (abstract). 21st Lunar and Planetary Science Conference pp. 932–933.

Paque J. M., Beckett J. R., Barber D. J., and Stolper E. M. 1994. A new titanium-bearing calcium aluminosilicate phase: I. Meteoritic occurrences and formation in synthetic systems. *Meteoritics* 29:673–682.

Paque J. M., Burnett D. S., and Beckett J. R. 2005. CAI thermal history constraints from spinel: Ti zoning profiles and melilite boundary clinopyroxenes (abstract #1809). 36th Lunar and Planetary Science Conference. CD-ROM.

Paque J. M., Burnett D. S., and Beckett J. R. 2007a. Zoning patterns of Fe and V in spinel from type B Ca-Al-rich inclusions: Constraints on subsolidus thermal history. *Meteoritics & Planetary Science* 42:899–912.

Paque J. M., Ishii H. A., Toppani A., Beckett J. R., Bradley J. P., Burnett D. S., Teslich N., and Moberlychan W. 2007b. Origin of boundary clinopyroxene between spinel and melilite in type B1 CAIs (abstract #5206). *Meteoritics & Planetary Science* 42: A121.

Paque J. M. and Stolper E. 1984. Crystallization experiments on a range of Ca-Al-rich inclusion compositions (abstract). 15th Lunar and Planetary Science Conference. pp. 631–632.

Paque J. M., Toppani A., Burnett D. S., Teslich N., Moberlychan W., Dai Z. R., and Bradley J. P. 2007c. TEM/SEM evidence for residual melt inclusions in type B1 CAIs (abstract #1755). 38th Lunar and Planetary Science Conference. CD-ROM.

Peters M. T., Shaffer E., Burnett D. S., and Kim S. S. 1995. Magnesium and titanium partitioning between anorthite and type B CAI liquid: Dependence on oxygen fugacity and liquid composition. *Geochimica et Cosmochimica Acta* 59:2785–2796.

Prenitzer B. I., Urbanik-Shannon C. A., Giannuzzi L. A., Brown S. R., Irwin R. B., Shofner T. L. and Stevie F. A. 2003. The correlation between ion beam/material interactions and practical FIB specimen preparation. *Microscopy and Microanalysis* 9: 216–236.

Reid A. M., Williams R. J., Gibson E. K., and Fredriksson K. 1974. A refractory glass chondrule in the Vigarano chondrite. *Meteoritics* 9:35–46.

Richter F. M. 2004. Time scales determining the degree of kinetic isotope fractionation by evaporation and condensation. *Geochimica et Cosmochimica Acta* 68:4971–4992.

Richter F. M., Davis A. M., Ebel D. S., and Hashimoto A. 2002. Elemental and isotopic fractionation of type B calcium-, aluminum-rich inclusions: Experiments, theoretical considerations, and constraints on their thermal evolution. *Geochimica et Cosmochimica Acta* 66:521–540.

Richter F. M., Mendybaev R. A., and Davis A. M. 2006. Conditions in the protoplanetary disk as seen by the type B CAIs. *Geochimica et Cosmochimica Acta* 41:83–93.

Rives V. 2001. *Layered double hydroxides: Present and future*. New York: Nova Science Publishers. 439 p.

Sharp T. G. and DeCarli D. S. 2006. Shock effects in meteorites. In *Meteorites and the early solar system II*, edited by D. S. Lauretta and H. Y. McSween. Tucson: The University of Arizona Press. 653–677 p.,

Sheng Y. J. 1992. The origin of plagioclase-olivine inclusions. Ph.D. thesis. California Institute of Technology, Pasadena, California, USA.

Sheng Y. J., Beckett J. R., Hutcheon I. D., and Wasserburg G. J. 1991. Experimental constraints on the origin of plagioclase-olivine inclusions and CA chondrules (abstract). 22nd Lunar and Planetary Science Conference. pp. 1231–1232.

Simon S. B., Davis A. M., and Grossman L. 1999. Origin of compact type A refractory inclusions from CV3 carbonaceous chondrites. *Geochimica et Cosmochimica Acta* 63:1233–1248.

Simon S. B. and Grossman L. 2006. A comparative study of melilite and fassaite in types B1 and B2 refractory inclusions. *Geochimica et Cosmochimica Acta* 70:780–798.

Simon S. B., Grossman L., and Davis A. M. 1991. Fassaite composition trends during crystallization of Allende type B refractory inclusion melts. *Geochimica et Cosmochimica Acta* 55:2635–2655.

Simon S. B., Grossman L., and Davis A. M. 2005. A unique type B inclusion from Allende with evidence for multiple stages of melting. *Meteoritics & Planetary Science* 40:461–475.

Stöffler D., Bischoff A., and Rubin A. E. 1988. Shock effects in meteorites. In *Meteorites and the early solar system*, edited by Kerridge J. F. and Matthews M. S. Tucson: The University of Arizona Press. pp. 165–202.

Stolper E. 1982. Crystallization sequences of Ca-Al-rich inclusions from Allende: An experimental study. *Geochimica et Cosmochimica Acta* 46:2159–2180.

Stolper E. and Paque J. M. 1986. Crystallization sequences of Ca-Al-rich inclusions from Allende: The effects of cooling rate and maximum temperature. *Geochimica et Cosmochimica Acta* 50: 1785–1806.

Stolper E., Paque J., and Rossman G. R. 1982. The influence of oxygen fugacity and cooling rate on the crystallization of Ca-Al inclusions from Allende (abstract). 13th Lunar and Planetary Science Conference. pp. 772–773.

Streck M. J. and Wacaster S. 2006. Plagioclase and pyroxene hosted melt inclusions in basaltic andesites of the current eruption of the Arenal volcano, Costa Rica. *Journal of Volcanology and Geothermal Research* 157:236–253.

Stroud R. M., Nittler L. R., and Alexander C. M. O. D. 2004. Polymorphism in presolar Al_2O_3 grains from asymptotic giant branch stars. *Science* 305:1455–1457.

Sylvester P. J., Simon S. B., and Grossman L. 1993. Refractory inclusions from the Leoville, Efremovka, and Vigarano C3V chondrites: Major element differences between types A and B, and extraordinary refractory siderophile element compositions. *Geochimica et Cosmochimica Acta* 57:3763–3784.

Toppani A., Paque J. M., Burnett D. S., Teslich N., Moberlychan W., Dai Z. R., and Bradley J. P. 2006. Wark-Lovering rims at the nanometer scale: a transmission electron microscopy study (abstract #2030). 37th Lunar and Planetary Science Conference. CD-ROM.

Vidal O., Parra T. and Trotet F. 2001. A thermodynamic model for Fe-Mg aluminous chlorite, using data from phase equilibrium experiments and natural pelitic assemblages in the 100 to 600 °C, 1 to 25 kb range. *American Journal of Science* 301:557–592.

Weber D. and Bischoff A. 1994. The occurrence of grossite ($CaAl_4O_7$) in chondrites. *Geochimica et Cosmochimica Acta* 58: 3855–3877.

Wei C. and Powell R. 2006. Calculated phase relations in the system NCKFMASH (Na_2O-CaO-K_2O-FeO-MgO-Al_2O_3-H_2O) for high-pressure metapelites. *Journal of Petrology* 47:385–408.

Wirth R. 1997. Water in minerals detectable by electron energy-loss spectroscopy EELS. *Physics and Chemistry of Minerals* 24:561–568.

Wlotzka F. and Wark D. A. 1982. The significance of zeolites and other hydrous alteration products in Leoville Ca-Al-rich inclusions (abstract). 13th Lunar and Planetary Science Conference. pp. 869–870.